Molecular Simulation
Vol. 35, Nos. 12–13, October–November 2009, 1098–1104

Taylor & Francis
Taylor & Francis Group

A molecular simulation study of commensurate–incommensurate adsorption of *n*-alkanes in cobalt formate frameworks

R. Krishna* and J.M. van Baten

Van't Hoff Institute for Molecular Sciences, University of Amsterdam, Amsterdam, The Netherlands

(*Received 9 December 2008; final version received 7 January 2009*)

The channels of the cobalt formate frameworks consist of one-dimensional channels that have a zig-zag configuration. Propane (C3) has a length that commensurates with the channel segment length; longer *n*-alkanes such as *n*-butane (*n*C4), *n*-pentane (*n*C5) and *n*-hexane (*n*C6) have conformations that straddle two channel segments. Configurational-bias Monte Carlo (CBMC) simulations show that the adsorption strength of C3 is higher than that of *n*-butane (*n*C4) and *n*-pentane (*n*C5); this unusual hierarchy is a direct consequence of the commensurate–incommensurate adsorption. CBMC simulations also reveal the possibility of separating C3–*n*C6, C3–*n*C4, *n*C4–*n*C6 and *n*C4–*n*C5 *liquid* mixtures for which the adsorbed phase contains predominantly the *shorter* alkane. Molecular dynamics simulations show that the hierarchy of self-diffusivities is non-monotonic and is the mirror image of the hierarchy of adsorption strengths.

Keywords: diffusivity; adsorption; molecular dynamics; configurational-bias Monte Carlo; linear alkanes; metal-organic frameworks; cobalt formate; manganese formate; commensurate; non-monotonous

1. Introduction

In recent years, there has been a remarkable upsurge in research activity on metal-organic frameworks (MOFs), in view of several potential applications in the field of storage [1–4], and also separation of a variety of mixtures [5–21]. Due to the wide variety of pore sizes and pore geometries, several interesting separation possibilities are possible with MOFs. For example, Finsy et al. [11] have reported a significantly higher adsorption capacity for xylene isomers in MIL-47, than for its isomers, *n*-octane (*n*C8) and ethyl benzene (EtBz). The higher capacity for xylene isomers is due to their improved 'stacking efficiency' within the channels of MIL-47, as illustrated in the snapshots in Figure 1(a), (b) for *p*-xylene and *n*C8, respectively; see also the pure-component isotherms in Figure 2. Bárcia et al. [7] report the results of an experimental study to show the feasibility of separating alkane isomers by adsorption within the framework of Zn(bdc)dabco (see the structure in Figure 3). In a subsequent study, Dubbeldam et al. [21] have used molecular simulations, which shown that the principle behind alkane isomers separation using Zn(bdc)dabco framework is based on the differences in 'efficiency' with which the isomer molecules can interact with the dabco linker atoms.

The current investigation focuses on another unusual separation potential of MOFs and has its genesis in the recent work by Li et al. [22], which reported adsorption isotherms for *n*-alcohols in cobalt formate (Co-FA) framework structure. The metal network exhibits diamondoid connectivity, and the overall framework gives rise to zigzag channels along the *b*-axis, where guest dimethylformamide molecules reside. The effective pore size of these one-dimensional channels is 5–6 Å. The unit cell and pore landscape of Co-FA is depicted in Figure 4; one unit cell of Co-FA comprises a total of four distinct channel 'segments'; each channel segment forms part of the repeat zigzag structure. The experimental adsorption data of Li et al. [22] for propanol and *n*-butanol in Co-FA are particularly intriguing (see Figure 5). We note that the adsorption strength of propanol is higher than that of *n*-butanol over the entire range of experimental pressures. The first major objective of the present communication is to show, with the help of molecular simulations, that this unusual hierarchy in adsorption strength is caused by commensurate–incommensurate molecular lengths of linear molecules within the one-dimensional channels of Co-FA. For this purpose, we have carried out a set of Configurational-bias Monte Carlo (CBMC) simulations to determine the adsorption isotherms of linear alkanes: methane (C1), ethane (C2), propane (C3), *n*-butane (*n*C4), *n*-pentane (*n*C5), *n*-hexane (*n*C6) and *n*-heptane (*n*C7) in Co-FA. The second objective is to demonstrate the exploitation of commensurate–incommensurate molecular lengths to adsorb a *shorter* linear alkane preferentially from a liquid mixture with a longer linear alkane. The third objective, using molecular dynamics (MD) diffusion of *n*-alkanes in Co-FA, is to show that the non-monotonous hierarchy of adsorption strengths is accompanied by a non-monotonous hierarchy in diffusivities.

*Corresponding author. Email: r.krishna@uva.nl

ISSN 0892-7022 print/ISSN 1029-0435 online

DOI: 10.1080/08927020902744672
http://www.informaworld.com

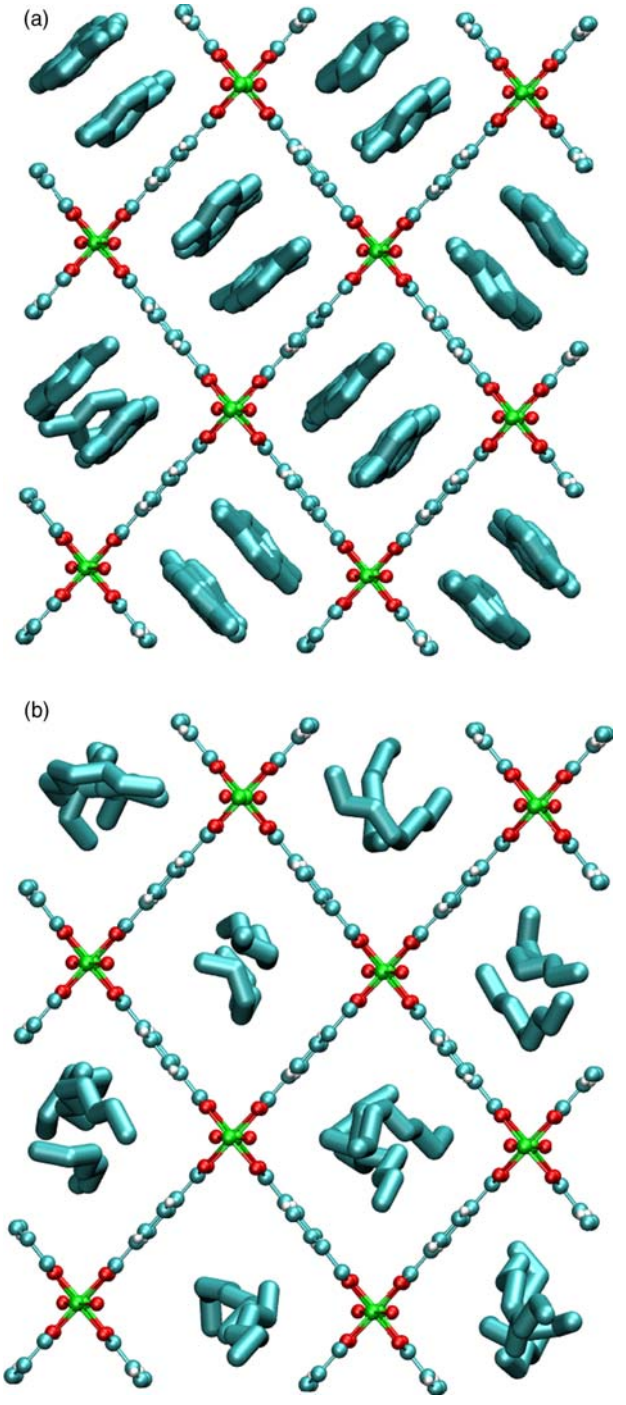

Figure 1. Snapshots showing the location and conformations of (a) *p*-xylene and (b) *n*C8 within the pores of MIL-47. The structural and simulation details are available in the supplementary material accompanying this publication.

2. Simulation details

The structural information for Co-FA is from Li et al. [22]. The adsorption isotherms were computed using CBMC simulations in the grand canonical ensemble. The united-atom force field for alkanes, developed by Dubbeldam et al. [23], is used to describe alkane–alkane, Lennard-Jones, interactions. For alkane–alkane interactions, the tabulated force fields are available in Dubbeldam et al. [23]; the potential for the *n*-alkanes includes bond stretching, bending and torsion. The framework was assumed to be rigid in the simulations.

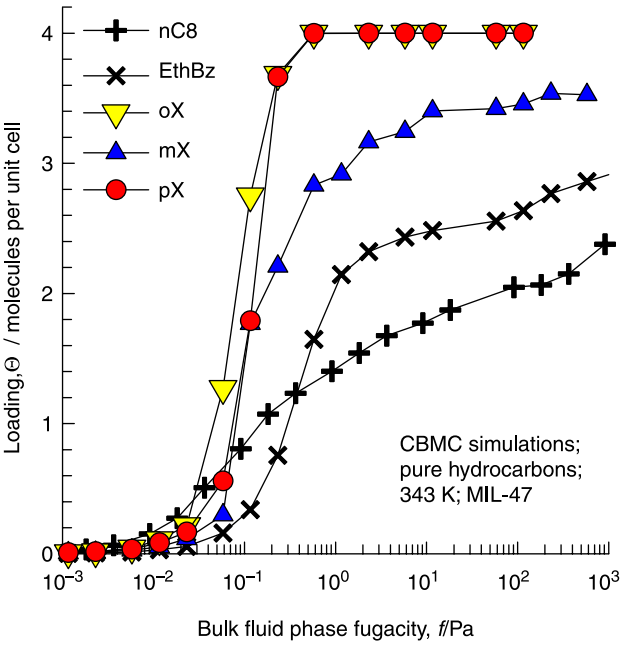

Figure 2. CBMC simulations of pure-component isotherms for *n*C8, EtBz, *o*-, *m*- and *p*-xylenes (*o* X, *m* X and *p* X) in MIL-47 at 343 K.

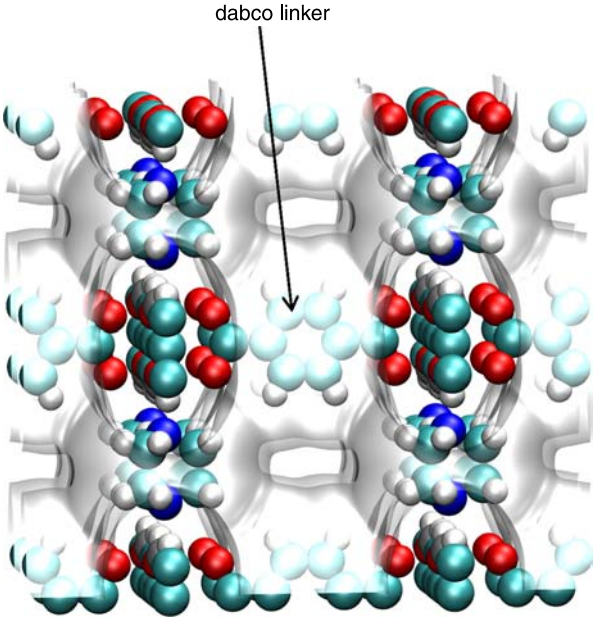

Figure 3. Pore landscape and structure of Zn(bdc)dabco. The structural and simulation details are available in the supplementary material accompanying this publication.

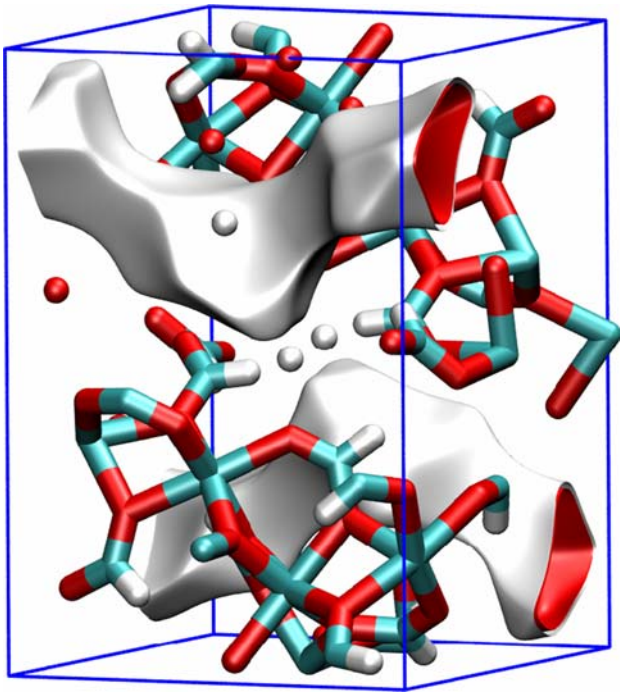

Figure 4. Pore landscapes and structure of Co-FA.

For the atoms in the guest metal-organic framework, the generic UFF [24] was used. The DREIDING [25] force field was used for the organic linker atoms. The Lorentz–Berthelot mixing rules were applied for calculating σ and ε/k_B for guest–host interactions.

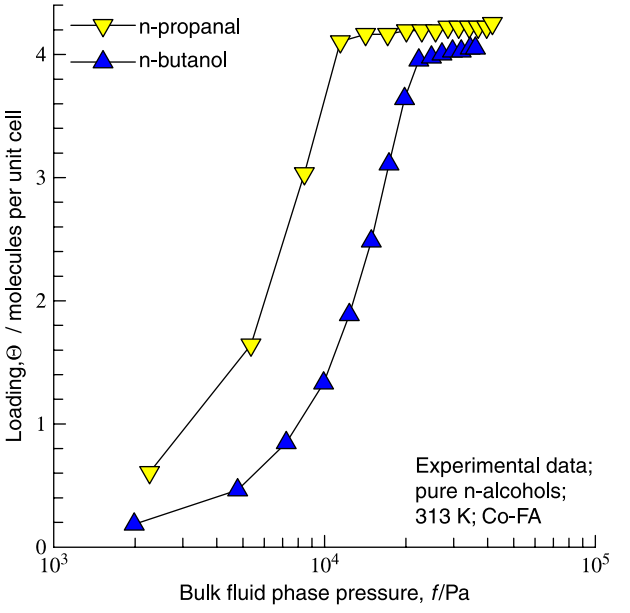

Figure 5. Adsorption isotherms for propanol and *n*-butanol in Co-FA. Experimental data of Li et al. [22]. See supplementary material for the unit cell dimensions and the conversion of loadings to units of molecules per unit cell.

Further simulation details, including structural information, CBMC and MD simulation methodologies, tabulated force fields, pore landscapes, snapshots showing the location and conformation of *n*-alkanes within the pores and simulation data are available in the Supplementary material accompanying this publication.

3. Adsorption of linear alkanes in Co-FA

Consider the CBMC simulations of the adsorption isotherms of linear alkanes in Co-FA at 300 K (see Figure 6(a)). The hierarchy of adsorption strengths for C1,

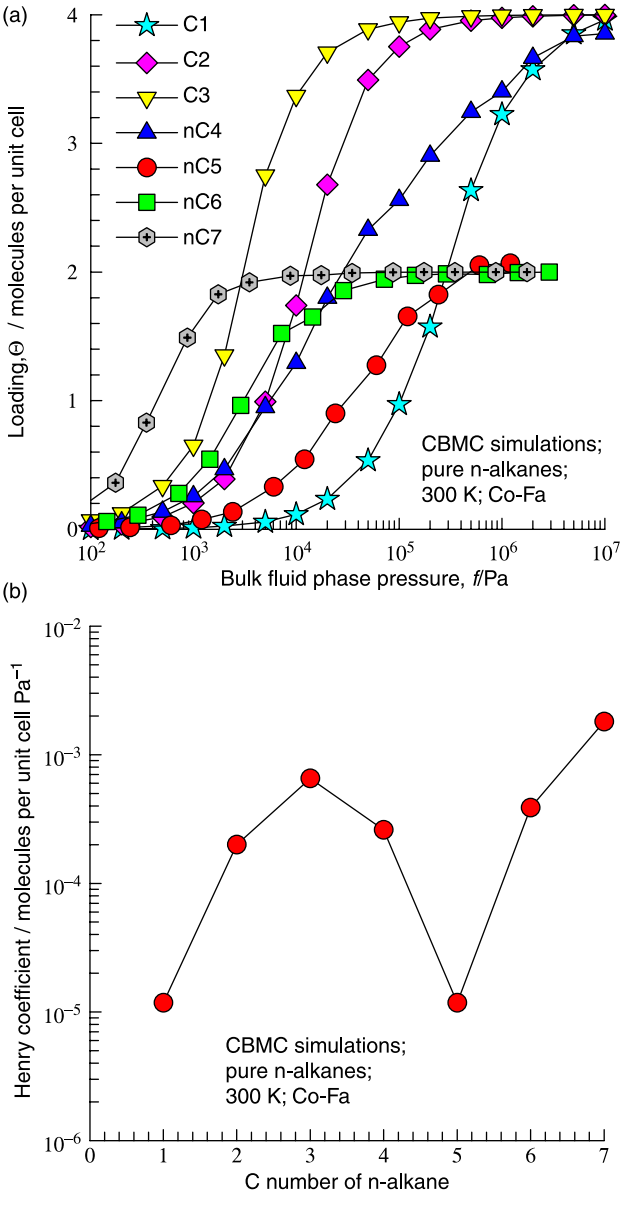

Figure 6. (a) CBMC simulations of adsorption isotherms for C1, C2, C3, *n*C4, *n*C5, *n*C6 and *n*C7 in Co-FA at 300 K. (b) Henry coefficients as a function of C number.

C2 and C3 is as expected; increasing chain length results in higher adsorption strength; see Henry coefficient data in Figure 6(b). However, with increasing chain lengths beyond C3 we note an unusual adsorption hierarchy: C3 > *n*C4 > *n*C5. Further increase in chain lengths result in the expected hierarchy, i.e. *n*C7 > *n*C6 > *n*C5. The saturation capacity for C1, C2 and C3 is found to be four molecules per unit cell, corresponding to one molecule per channel segment. Snapshots of the location of molecules along the one-dimensional zigzag channels of Co-FA confirm that each channel segment contains no more than one molecule each of C1, C2 and C3 (see Figure 7). *n*C5, *n*C6 and *n*C7 have conformations that make these molecules straddle two channel segments, and this is also reflected in the saturation capacities of these molecules of two molecules per unit cell, i.e. corresponding to one molecule in two channel segments. *n*C4 has an intermediate character; at low pressures, the *n*C4 has a conformation with a tendency to occupy a small portion of the adjoining segment. At very high pressures, *n*C4 adopts a more 'cramped' configuration, with each molecule occupying one channel segment and yielding a saturation capacity of four molecules per unit cell. When a molecule has a tendency to straddle two channel segments (*n*C4 at low pressures, *n*C5, *n*C6 and *n*C7), not all of the C atoms can effectively interact with the atoms of the framework; this leads to lower adsorption strength and a non-monotonous adsorption hierarchy witnessed in the Henry coefficient data in Figure 6(b). It is interesting to note that non-monotonous behaviour of the Henry coefficient for *n*-alkanes has also been observed for cage-type zeolites such as CHA, ERI and LTA, caused by commensurate–incommensurate adsorption within cages [26–28].

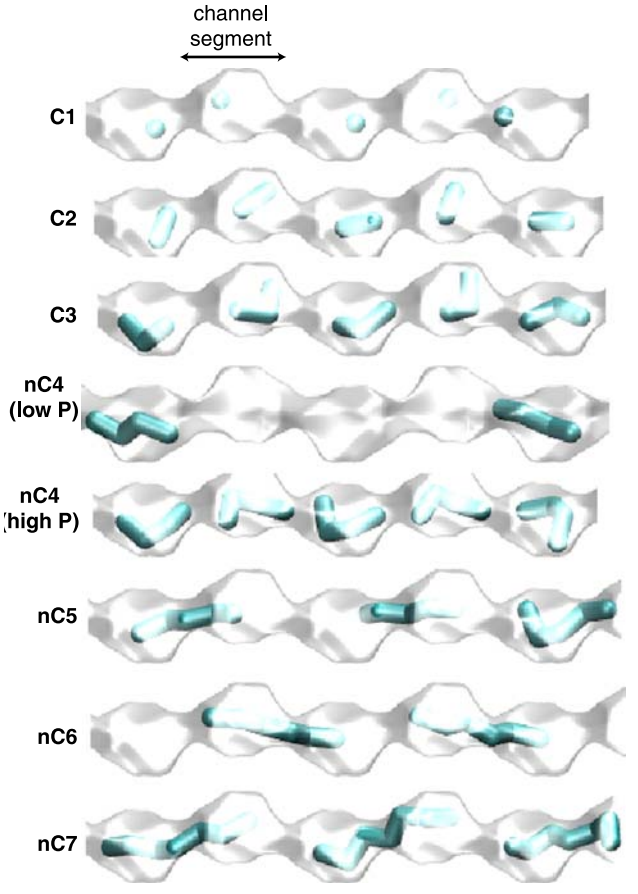

Figure 7. Snapshots showing the location of C1, C2, C3, *n*C4, *n*C5, *n*C6 and *n*C7 molecules in Co-FA.

The non-monotonous adsorption characteristics, along with differences in saturation capacities, can be exploited to achieve unusual separation possibilities. Consider a mixture of C3 and *n*C6. From the pure-component adsorption isotherms in Figure 6 we note that at low pressures the adsorption strengths of C3 is nearly the same as that of *n*C6. However, the saturation capacity of C3 is twice that of *n*C6. We can device a strategy for separating C3 from *n*C6 by exploiting the differences in the saturation capacities. CBMC simulations of the component loadings for a mixture with equal partial fluid phase fugacities, $f_1 = f_2$, are shown in Figure 8(a). When operating at partial fugacities in excess of 1 MPa, with a bulk *liquid* phase, we note that the adsorbed phase contains practically no *n*C6 and is predominantly C3.

Analogously, for *n*C4–*n*C5 liquid mixtures, the adsorbed phase contains the shorter alkane, almost exclusively (see Figure 8(b)). For the C3–*n*C4 and *n*C4–*n*C6 mixtures the separation is somewhat less selective. The CBMC simulation results in Figure 9 show that at high loadings the adsorbed phase is not exclusively the shorter alkane but also contains a small proportion of the longer alkane. The separations indicated in Figures 8 and 9 have possible industrial potential, and needs to be experimentally confirmed. It is perhaps relevant to point out here that earlier we had used molecular simulations to demonstrate the feasibility of separating *n*-alkane mixtures by exploiting differences in the saturation capacity in cage-type zeolites such as CHA, ERI and AFX zeolites [29]. More recently, the experimental work of Denayer et al. [30] has provided experimental confirmation of the separation potential anticipated by the molecular simulations.

4. Diffusion of linear alkanes in Co-FA

MD simulations of self-diffusivities of C1, C2, C3, *n*C4, *n*C5, *n*C6 and *n*C7 in Co-FA are shown in Figure 10(a) for a variety of loadings. At a loading of one molecule per unit cell, the values of the self-diffusivities are plotted in Figure 10(b) as a function of C number. The hierarchy of diffusivities of C1, C2 and C3 is as expected; the molecule with the longer chain length has the lower diffusivity. With increasing chain length, we observe a non-monotonous

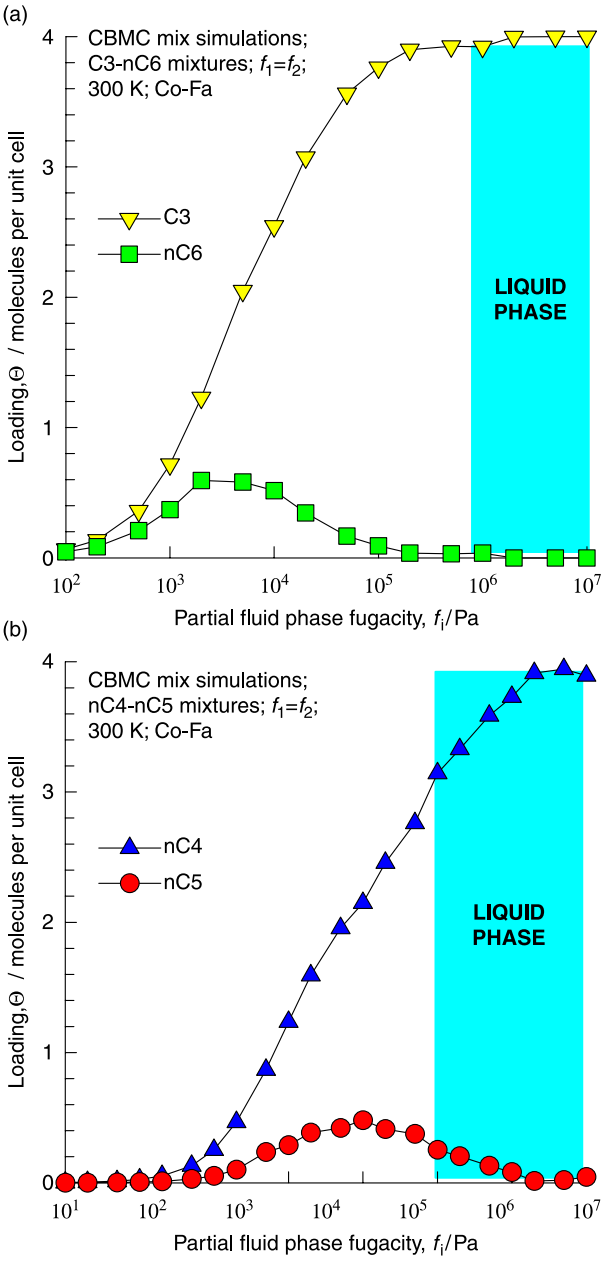

Figure 8. CBMC simulations of component loadings for (a) C3–*n*C6 and (b) *n*C4–*n*C5 mixtures in Co-FA at 300 K.

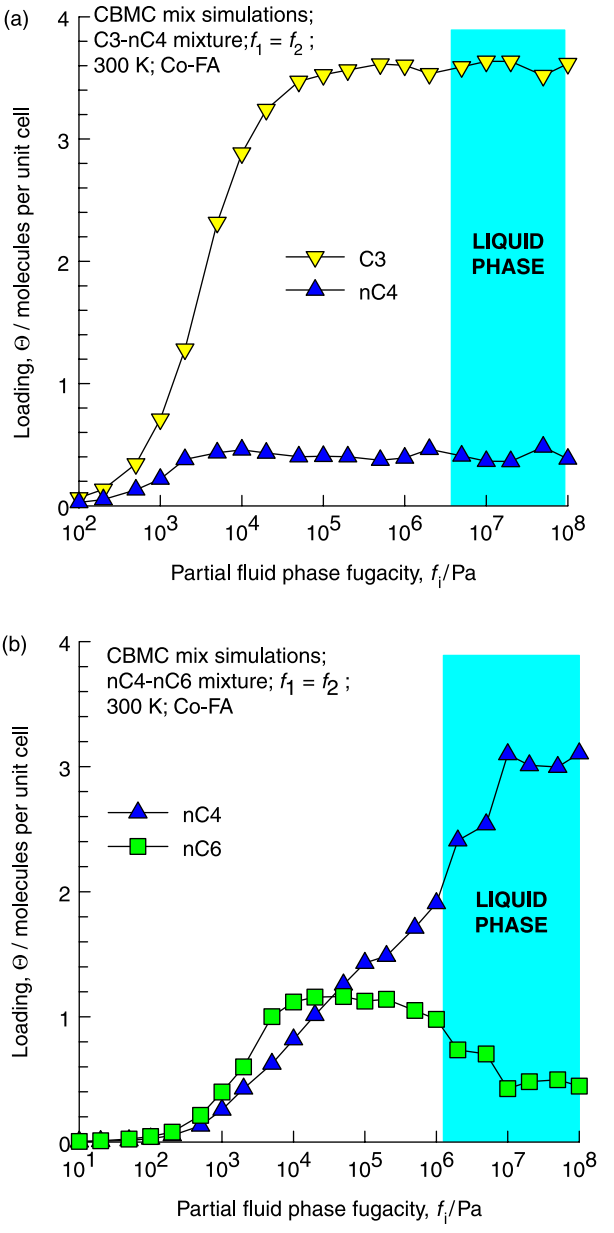

Figure 9. CBMC simulations of component loadings for (a) C3–*n*C4 and (b) *n*C4–*n*C6 mixtures in Co-FA at 300 K.

behaviour with the hierarchy: *n*C5 > *n*C4 > C3 ≈ *n*C6. The hierarchy of diffusivities is an exact mirror image of the hierarchy of Henry coefficients (compare Figures 6(b) and 10(b)). Put another way, if the molecular length is incommensurate with the channel segment length, the adsorption strength is low, but its diffusivity is high.

In the context of separation process development, it must be emphasized that since adsorption and diffusion run counter to each other, we should aim for either an equilibrium- or a diffusion- (i.e. kinetic) based separation. A combination of the two, for example, in a MOF membrane separation will not work, as the two effects may cancel each other out.

5. Conclusions

CBMC and MD simulations of adsorption and diffusion of linear alkanes within the one-dimensional channels of cobalt formate frameworks have revealed a non-monotonic behaviour in Henry coefficients and diffusivities as a function of the *n*-alkane chain length. The non-monotonicity is caused due to commensurate–incommensurate effects in adsorption; C3 has a molecular length that

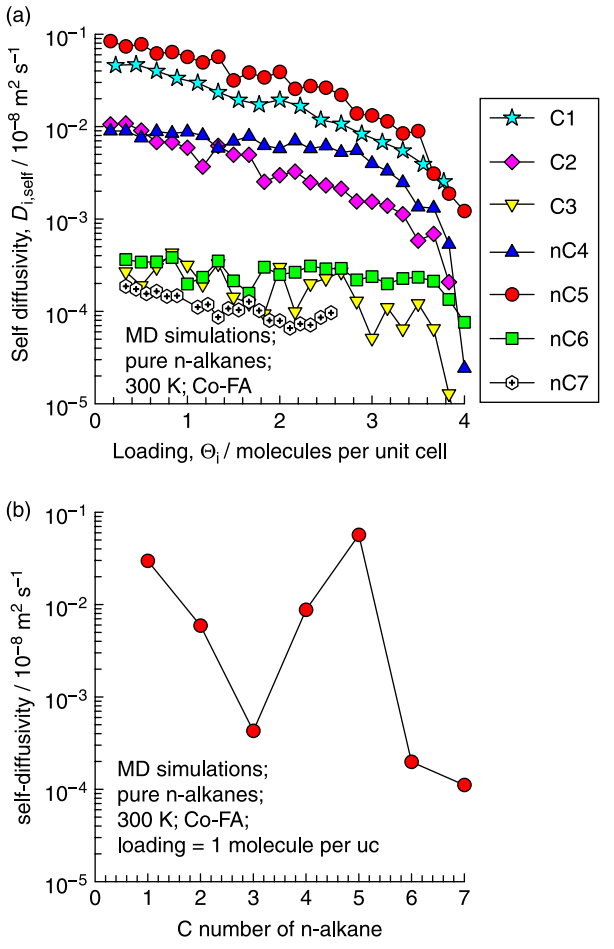

Figure 10. (a) MD simulations of self-diffusivities of C1, C2, C3, *n*C4, *n*C5, *n*C6 and *n*C7 in Co-FA at 300 K. (b) Diffusivities, at a loading of one molecule per unit cell, as a function of carbon number.

commensurates with the channel segment length. *n*C4, *n*C5, *n*C6 and *n*C7 have conformations that make these molecules straddle two channel segments; this leads to lower adsorption strength due to inefficient interaction with the framework atoms. The hierarchy of diffusivities is inverse of the hierarchy of adsorption strengths.

CBMC simulations also reveal the possibility of separating C3–*n*C6, C3–*n*C4, *n*C4–*n*C6 and *n*C4–*n*C5 *liquid* mixtures for which the adsorbed phase contains predominantly the *shorter* alkane.

Manganese formate frameworks are isostructural to Co-FA, and a similar non-monotonicity in adsorption and diffusion behaviours is observed from molecular simulations; details are available in the supplementary material.

Our study underlines the ability of molecular simulations to provide a molecular-level understanding of observed experimental phenomena, and also to unravel novel separations with structured nanoporous materials such as MOFs.

Supplementary material

Supplementary material associated with this article can be found with the online version at the journal's website.

Acknowledgements

RK acknowledges the grant of a TOP subsidy from The Netherlands Foundation for Fundamental Research (NWO-CW) for intensification of reactors.

References

[1] O.M. Yaghi, M. O'Keeffe, N.W. Ockwig, H.K. Chae, M. Eddaoudi, and J. Kim, *Reticular synthesis and the design of new materials*, Nature 423 (2003), pp. 705–714.

[2] J.L.C. Rowsell and O.M. Yaghi, *Metal-organic frameworks: a new class of porous materials*, Micropor. Mesopor. Mater. 73 (2004), pp. 3–14.

[3] O.M. Yaghi, *Metal-organic frameworks: a tale of two entanglements*, Nat. Mater. 6 (2007), pp. 92–93.

[4] R.Q. Snurr, J.T. Hupp, and S.T. Nguyen, *Prospects for nanoporous metal-organic materials in advanced separations processes*, AIChE J. 50 (2004), pp. 1090–1095.

[5] L. Bastin, P.S. Bárcia, E.J. Hurtado, J.A.C. Silva, A.E. Rodrigues, and B. Chen, *A microporous metal-organic framework for separation of CO_2/N_2 and CO_2/CH_4 by fixed-bed adsorption*, J. Phys. Chem. C 112 (2008), pp. 1575–1581.

[6] L. Pan, D.H. Olson, L.R. Ciemnolonski, R. Heddy, and J. Li, *Separation of hydrocarbons with a microporous metal-organic framework*, Angew. Chem. Int. Ed. 45 (2006), pp. 616–619.

[7] P.S. Bárcia, F. Zapata, J.A.C. Silva, A.E. Rodrigues, and B. Chen, *Kinetic separation of hexane isomers by fixed-bed adsorption with a microporous metal-organic framework*, J. Phys. Chem. B 111 (2008), pp. 6101–6103.

[8] B. Chen, C. Liang, J. Yang, D.S. Contreras, Y.L. Clancy, E.B. Lobkovsky, O.M. Yaghi, and S. Dai, *A microporous metal-organic framework for gas-chromatographic separation of alkanes*, Angew. Chem. Int. Ed. 45 (2006), pp. 1590–1595.

[9] L. Pan, B. Parker, X. Huang, D.H. Olson, J.Y. Lee, and J. Li, *Zn(tbip) (H_2 tbip) = 5-tert-butyl isophthalic acid): a highly stable guest-free microporous metal organic framework with unique gas separation capability*, J. Am. Chem. Soc. 128 (2006), pp. 4180–4181.

[10] D.N. Dybtsev, H. Chun, S.H. Yoon, D. Kim, and K. Kim, *Microporous manganese formate: a simple metal-organic porous material with high framework stability and highly selective gas sorption properties*, J. Am. Chem. Soc. 126 (2004), pp. 32–33.

[11] V. Finsy, H. Verelst, L. Alaerts, D. De Vos, P.A. Jacobs, G.V. Baron, and J.F.M. Denayer, *Pore-filling-dependent selectivity effects in the vapor-phase separation of xylene isomers on the metal-organic framework MIL-47*, J. Am. Chem. Soc. 130 (2008), pp. 7110–7118.

[12] L. Alaerts, C.E.A. Kirschhock, M. Maes, M. van der Veen, V. Finsy, A. Depla, J.A. Martens, G.V. Baron, P.A. Jacobs, J.F.M. Denayer et al., *Selective adsorption and separation of xylene isomers and ethylbenzene with the microporous vanadium(IV) terephthalate MIL-47*, Angew. Chem. Int. Ed. 46 (2007), pp. 4293–4297.

[13] Q.M. Wang, D. Shen, M. Bülow, M.L. Lau, S. Deng, F.R. Fitch, N.O. Lemcoff, and J. Semanscin, *Metallo-organic molecular sieve for gas separation and purification*, Micropor. Mesopor. Mater. 55 (2002), pp. 217–230.

[14] L. Zhang, Q. Wang, T. Wu, and Y.C. Liu, *Understanding adsorption and interactions of alkane isomer mixtures in isoreticular metal-organic frameworks*, Chem. Eur. J. 13 (2007), pp. 6387–6396.

[15] S. Wang, Q. Yang, and C. Zhong, *Adsorption and separation of binary mixtures in a metal-organic framework Cu-BTC: a computational study*, Sep. Purif. Technol. 60 (2008), pp. 30–35.

[16] Q. Yang, C. Xue, C. Zhong, and J.F. Chen, *Molecular simulation of separation of CO_2 from flue gases in Cu-BTC metal-organic framework*, AIChE J. 53 (2007), pp. 2832–2840.

[17] Q. Yang and C. Zhong, *Molecular simulation of carbon dioxide/methane/hydrogen mixture adsorption in metal-organic frameworks*, J. Phys. Chem. B 110 (2006), pp. 17776–17783.

[18] S. Keskin and D.S. Sholl, *Screening metal-organic framework materials for membrane-based methane/carbon dioxide separations*, J. Phys. Chem. C 111 (2007), pp. 14055–14059.

[19] J. Jiang and S.I. Sandler, *Monte Carlo simulation for the adsorption and separation of linear and branched alkanes in IRMOF-1*, Langmuir 22 (2006), pp. 5702–5707.

[20] R. Babarao, Z. Hu, J. Jiang, S. Chempath, and S.I. Sandler, *Storage and separation of CO_2 and CH_4 in silicalite, C_{168} schwarzite, and IRMOF-1: a comparative study from Monte Carlo simulation*, Langmuir 23 (2007), pp. 659–666.

[21] D. Dubbeldam, C.J. Galvin, K.S. Walton, D.E. Ellis, and R.Q. Snurr, *Separation and molecular-level segregation of complex alkane mixtures in metal-organic frameworks*, J. Am. Chem. Soc. 130 (2008), pp. 10884–10885.

[22] K. Li, D.H. Olson, J.Y. Lee, W. Bi, K. Wu, T. Yuen, Q. Xu, and J. Li, *Multifunctional microporous MOFs exhibiting gas/hydrocarbon adsorption selectivity, separation capability and three-dimensional magnetic ordering*, Adv. Funct. Mater. 18 (2008), pp. 2205–2214.

[23] D. Dubbeldam, S. Calero, T.J.H. Vlugt, R. Krishna, T.L.M. Maesen, and B. Smit, *United atom forcefield for alkanes in nanoporous materials*, J. Phys. Chem. B 108 (2004), pp. 12301–12313.

[24] A.K. Rappé, C.J. Casewit, K.S. Colwel, W.A. Goddard, and W.M. Skiff, *UFF, a full periodic table force field for molecular mechanics and molecular dynamics simulations*, J. Am. Chem. Soc. 114 (1992), pp. 10024–10035.

[25] S.L. Mayo, B.D. Olafson, and W.A. Goddard, *DREIDING: a generic force field for molecular simulations*, J. Phys. Chem. 94 (1990), pp. 8897–8909.

[26] D. Dubbeldam, S. Calero, T.L.M. Maesen, and B. Smit, *Understanding the window effect in zeolite catalysis*, Angew. Chem. Int. Ed. 42 (2003), pp. 3624–3626.

[27] D. Dubbeldam, S. Calero, T.L.M. Maesen, and B. Smit, *Incommensurate diffusion in confined systems*, Phys. Rev. Lett. 90(24) (2003), 245901.

[28] D. Dubbeldam and B. Smit, *Computer simulation of incommensurate diffusion in zeolites: understanding window effects*, J. Phys. Chem. B 107 (2003), pp. 12138–12152.

[29] R. Krishna and J.M. van Baten, *Separating* n*-alkane mixtures by exploiting differences in the adsorption capacity within cages of CHA, AFX and ERI zeolites*, Sep. Purif. Technol. 60 (2008), pp. 315–320.

[30] J.F.M. Denayer, L.I. Devriese, S. Couck, J.A. Martens, R. Singh, P.A. Webley, and G.V. Baron, *Cage and window effects in the adsorption of* n*-alkanes on chabazite and SAPO-34*, J. Phys. Chem. C 112 (2007), pp. 16593–16599.

Molecular Simulation
1–24

Taylor & Francis
Taylor & Francis Group

Supplementary Material

A molecular simulation study of commensurate–incommensurate adsorption of *n*-alkanes in cobalt formate frameworks

R. Krishna, J.M. van Baten

Van't Hoff Institute for Molecular Sciences, University of Amsterdam, Amsterdam, The Netherlands

1. MOF structures

Besides cobalt formate frameworks, simulations were also carried out for manganese formate (Mn-FA), Zn(bdc)dabco and MIL-47. The structural information for the metal-organic frameworks have been taken from various publications on the respective frameworks: cobalt formate (Co-FA) from Li et al. [1]; manganese formate (Mn-FA) from Dybtsev et al. [2]; Zn(bdc)dabco from Bárcia et al. [3] and Lee et al. [4]; and MIL-47 from Alaerts et al. [5], Finsy et al. [6] and Barthelet et al. [7]. The structure data files we used in our simulations are available on our web site [8].

2. Monte Carlo simulation methodology

The adsorption isotherms were computed using Configurational-bias Monte Carlo (CBMC) simulations in the grand canonical ensemble. The united-atom force field for alkanes, developed by Dubbeldam et al. [9], is used to describe alkane–alkane, Lennard-Jones, interactions. For alkane–alkane interactions, the tabulated force fields are available in Dubbeldam et al. [9]; the potential for the *n*-alkanes includes bond stretching, bending and torsion. Some simulation results have also been reported for aromatics and alkyl aromatics in MIL-47. The force field for benzene follows the work of Ban et al. [10], and is extended to alkyl aromatics by combining with the force field of Dubbeldam et al. [9].

The metal-organic framework structures of Co-FA, Mn-FA, Zn(bdc)dabco and MIL-47 were considered to be rigid in the simulations. For the atoms in the guest metal-organic framework, the generic UFF [11] was used. The DREIDING [12] force fields were used for the organic linker atoms. The Lennard-Jones parameters are summarised in Table S1. The Lorentz–Berthelot mixing rules were applied for calculating (σ and ε/k_B for guest–host interactions. For simulations with linear and branched alkanes with two or more C atoms, the Configurational-bias Monte Carlo (CBMC) simulation technique [13,14] was employed. The beads in the chain are connected by harmonic bonding potentials. A harmonic cosine bending potential models the bond bending between three neighbouring beads, a Ryckaert–Bellemans potential controls the torsion angle. The beads in a chain separated by more than three bonds interact with each other through a Lennard-Jones potential. The Lennard-Jones potentials are shifted and cut at 12 Å. The CBMC simulation details have been given in detail elsewhere [9,13–15]. The CBMC simulations were performed using the BIGMAC code developed by Vlugt [16] as basis.

3. MD simulation methodology

Diffusion of linear alkanes in Co-FA and Mn-FA were investigated and simulated using Newton's equations of motion until the system properties, on average, no longer change in time. The Verlet algorithm is used for time integration. A time step of 1 fs was used in all simulations. For each simulation, *initialising* CBMC moves are used to place the molecules in the domain, minimising the energy. Next, follows an *equilibration* stage. These are essentially the same as the production cycles, only the statistics are not yet taken into account. This removes any initial large disturbances in the system that does not affect the statistics on molecular displacements. After a fixed number of initialisation and equilibrium steps, the MD simulation *production* cycles start. For every cycle, the statistics for determining the mean square displacements (MSDs) are updated. The MSDs are determined for time intervals ranging from 2 fs to 1 ns. In order to do this, an order-*N* algorithm, as detailed in Chapter 4 of Frenkel and Smit [13] is implemented. The Nose–Hoover thermostat is applied to all the diffusing particles.

The DLPOLY code [17] was used along with the force field implementation as described in the previous section. DLPOLY is a molecular dynamics simulation package written by Smith, Forester and Todorov and has been obtained from CCLRCs Daresbury Laboratory via the web site [17].

The MD simulations were carried out for a variety of molecular loadings. All simulations were carried out on the LISA clusters of PCs equipped with Intel Xeon processors running at 3.4 GHz on the Linux operating system [18]. Each MD simulation, for a specified loading, was run for 120 h, determined to be long enough to obtain reliable statistics for the determination of the diffusivities. In many cases, several independent MD simulations were run and the results were averaged.

The self-diffusivities, $D_{i,\text{self}}$, were computed by analysing the mean square displacement of each species i for each of

Table S1. Lennard-Jones parameters for atoms in metal–organic host framework.

(Pseudo-) atom	σ (Å)	ε/k_B (K)
Cu	3.114	2.518
Zn	2.69	0.41
Co	2.56	7.046
Mn	2.638	6.543
O	3.03	48.19
C	3.47	47.86
N	3.26	38.95
H	2.85	7.65

For the atoms in the guest metal organic framework, the generic UFF [11] was used. The DREIDING [12] force fields was used for the organic linker atoms.

Table S2. Dimensions of unit cell, along with factor to convert loadings from molecules per unit cell to mol per kg of framework.

MOF	*a* (Å)	*b* (Å)	*c* (Å)	Conversion factor
Co-FA	11.3834	9.9292	14.4324	0.56
Mn-FA	11.715	10.248	15.159	0.575
MIL-47	6.808	16.12	13.917	1.08
Zn(bdc)dabco	10.9288	10.9288	9.6084	1.75

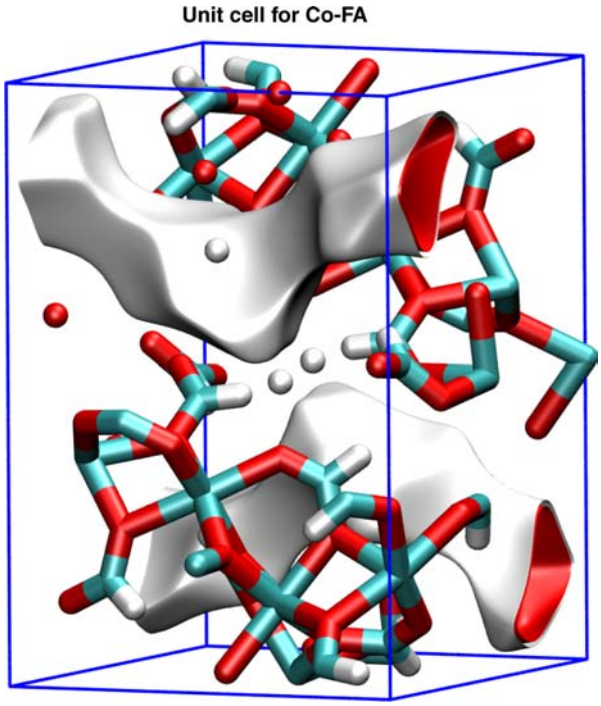

Figure S1.

the coordinate directions:

$$D_{i,\text{self}} = \frac{1}{2n_i} \lim_{\Delta t \to \infty} \frac{1}{\Delta t} \left\langle \left(\sum_{l=1}^{n_i} (\boldsymbol{r}_{l,i}(t + \Delta t) - \boldsymbol{r}_{l,i}(t))^2 \right) \right\rangle. \quad (1)$$

In this expression, n_i represents the number of molecules of species i, respectively, and $\mathbf{r}_{l,i}(t)$ is the position of molecule l of species i at any time t. For one-dimensional pore structures of Mn-FA and Co-FA, the diffusivities along the y-direction of diffusion are reported.

4. Animations

For visual appreciation of the diffusion phenomena in Co-FA, Mn-FA, Zn(bdc)dabco and MIL-47, animations were created on the basis of the MD simulations; these can be viewed by downloading the movies from our web site [8].

5. Simulation results for Co-FA

Figures S1–10 present the pore landscapes and snapshots of *n*-alkanes in Co-FA. The simulation results, summarised in Figure S11, have been discussed in the main text of the paper.

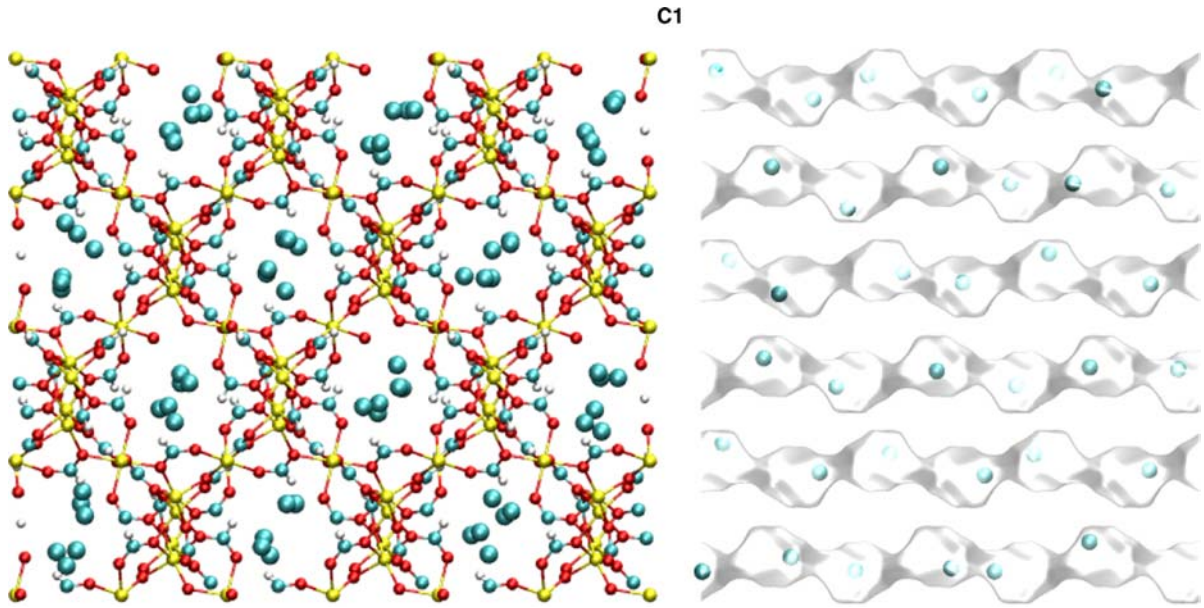

Figure S2.

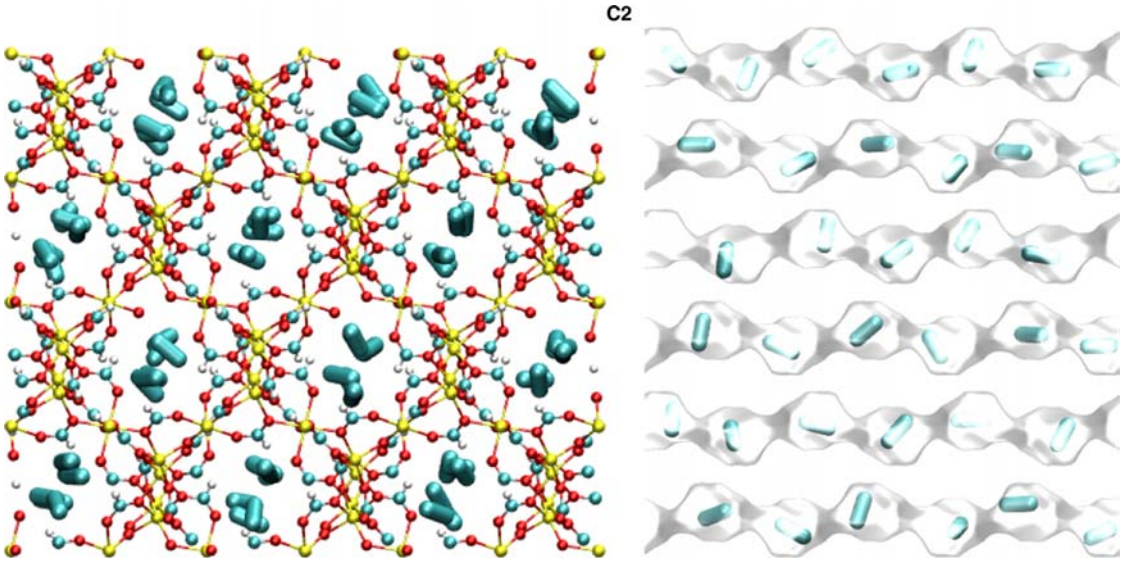

Figure S3.

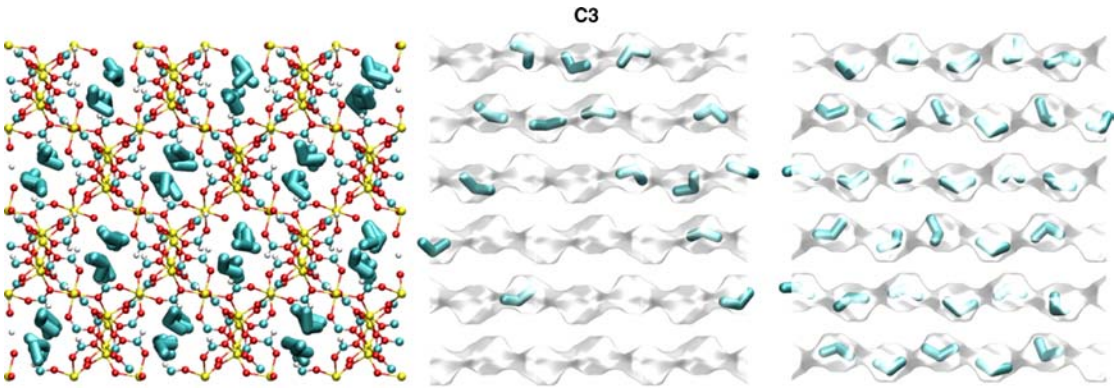

Figure S4.

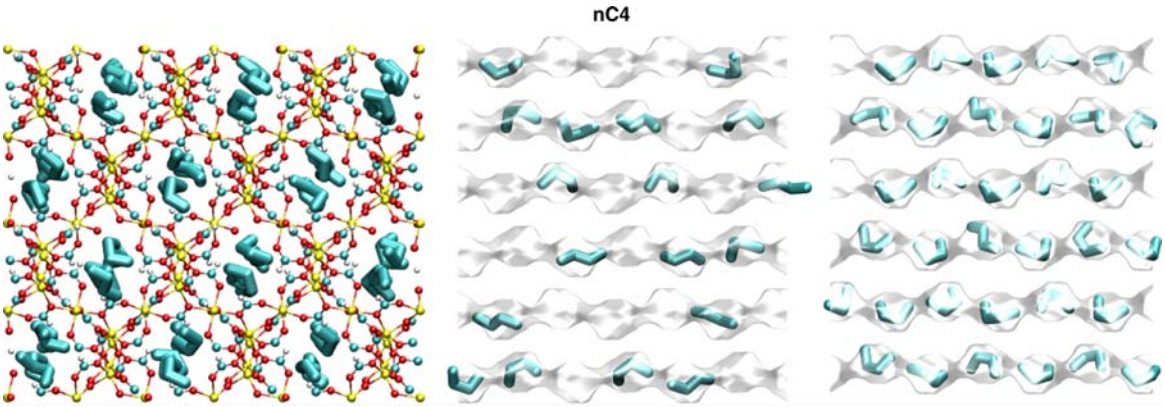

Figure S5.

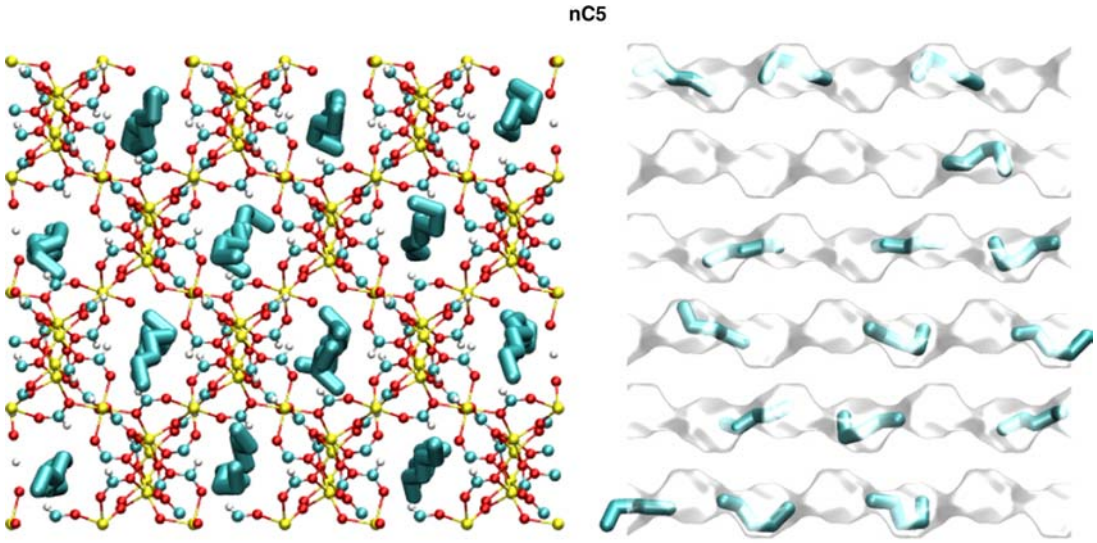

Figure S6.

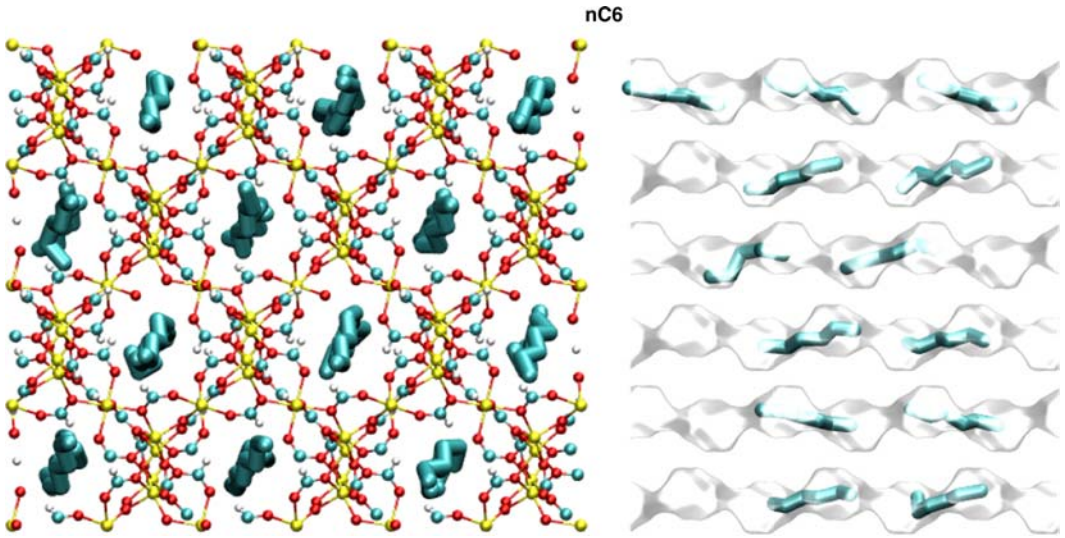

Figure S7.

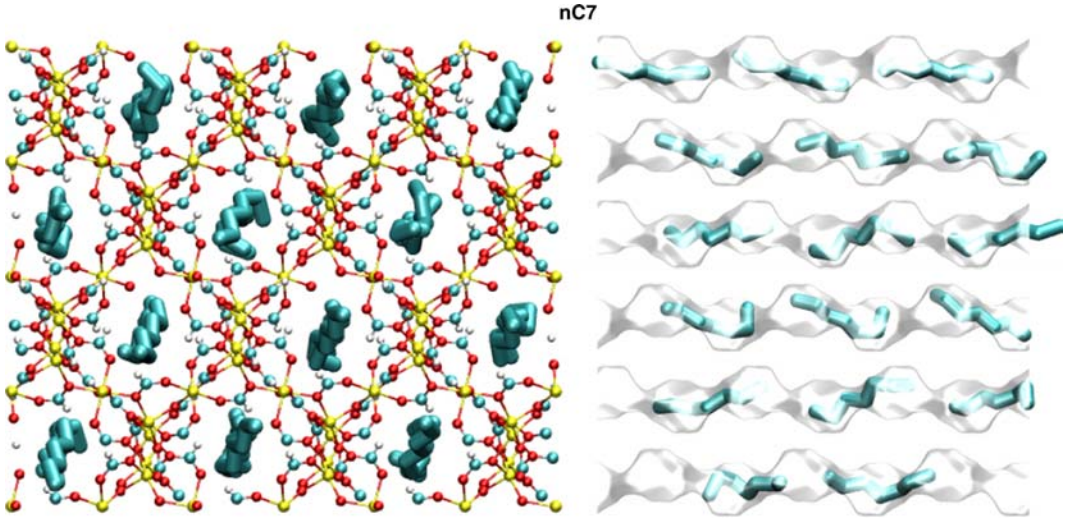

Figure S8.

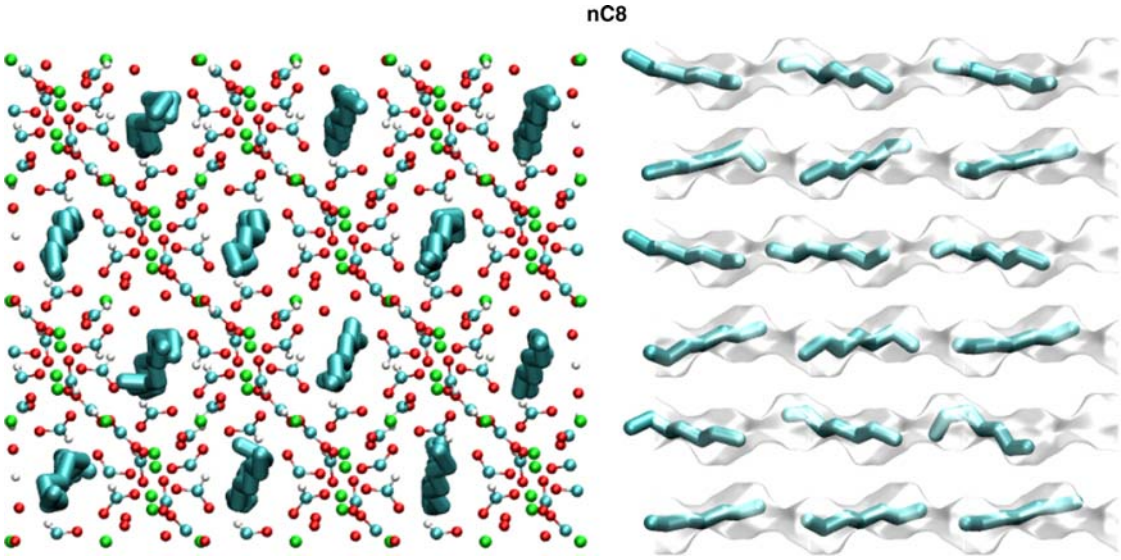

Figure S9.

6. Simulation results for Mn-FA

Figures S12–21 present the pore landscapes and snapshots of *n*-alkanes in Mn-FA. The simulation results for adsorption of *n*-alkanes. As with Co-FA, the adsorbed phase is predominantly the shorter alkane. The near-complete separation of the *n*C4–*n*C5 mixture at high loadings is particularly noteworthy. The diffusivity data for *n*-alkanes is summarised in Figure S22. Again we note the non-monotonicity as for Co-FA.

7. Simulation results for MIL-47

Figures S24–32 present the pore landscapes and snapshots for xylenes, *n*C8, ethyl benzene and benzene within the channels of MIL-47. In Figure S33, the CBMC simulations of the pure component isotherms for C8 isomers are compared with the experimental results of Finsy et al. [6]. There is reasonably good agreement in the saturation capacities, and the results indicate the possibility of separating C8 hydrocarbon isomers using differences in 'stacking' efficiency within the channels of MIL-47.

8. Simulation results for Zn(bdc)dabco

Figures S34–45 present the pore landscapes and snapshots of a variety of alkanes in Zn(bdc)dabco. Pure component, and ternary, CBMC simulations of the isotherms for *n*C6, 3MP and 22DMB are present in Figure S46. The simulations at 300 K are in good agreement with the simulation results of Dubbeldam et al. [19]. Also shown in Figure S46 are the comparisons of the pure component isotherms for hexane isomers at 313 K obtained from CBMC simulations (top right) with the experimental data of Bárcia et al. [3] (bottom right). The agreement is very poor. We suspect that in the experiments the Zn(bdc) dabco structure must have undergone phase transition because the reported experimental loadings are about one order of magnitude lower than the usual loading values found for MOFs.

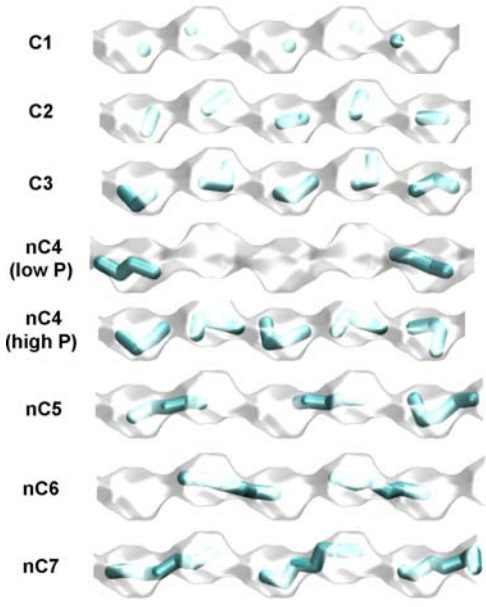

Figure S10.

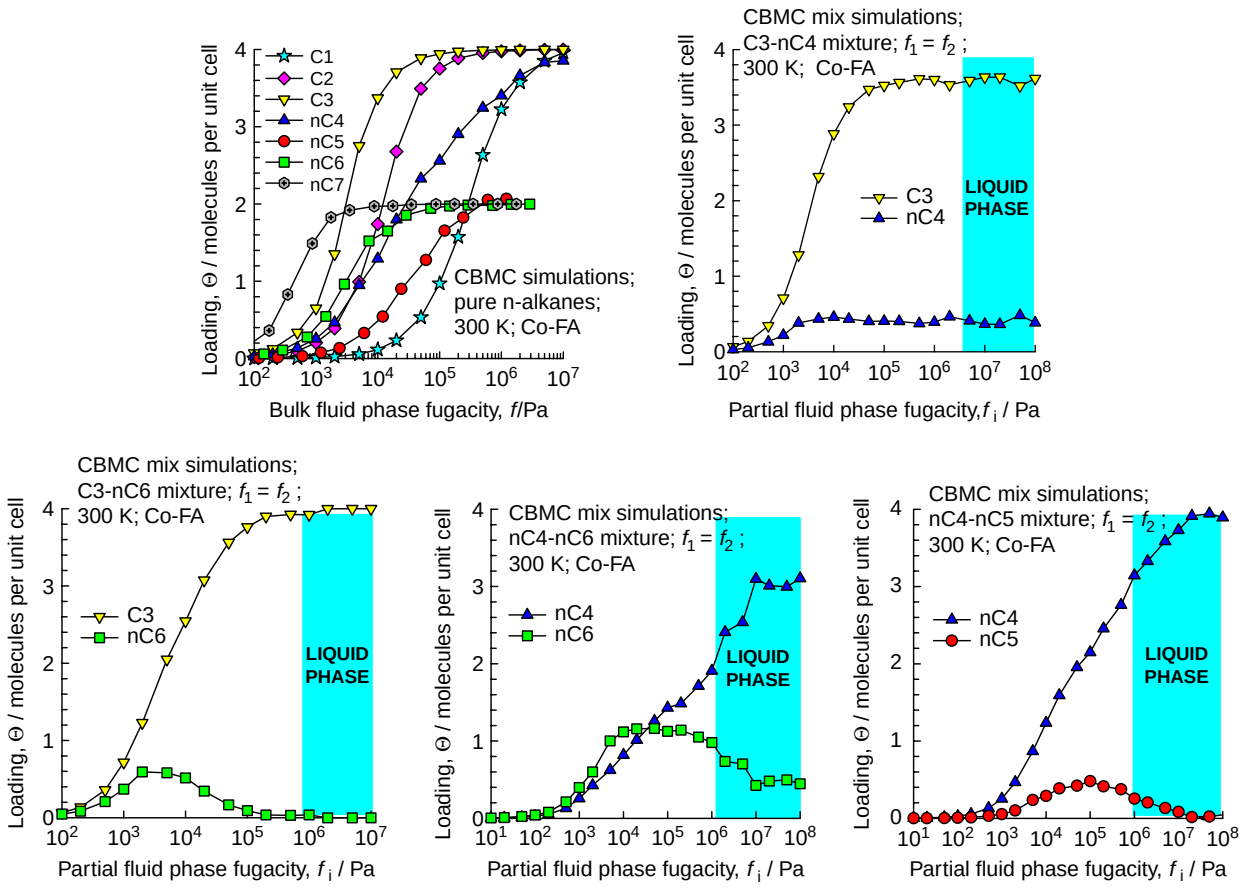

Figure S11.

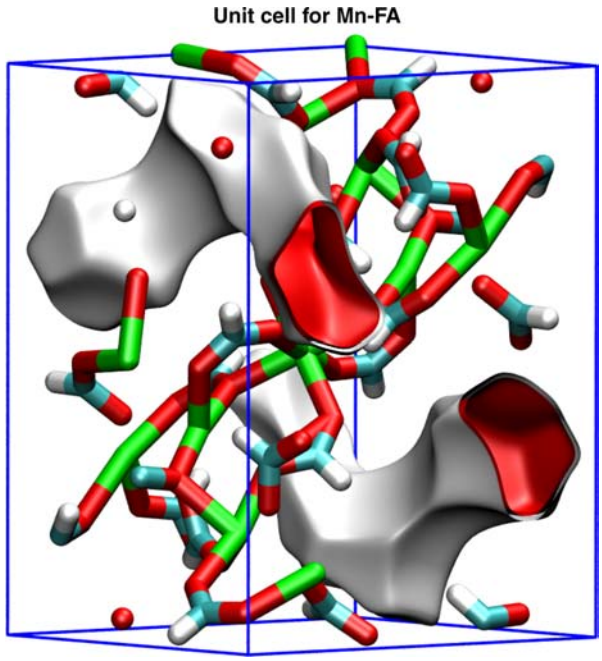

Figure S12.

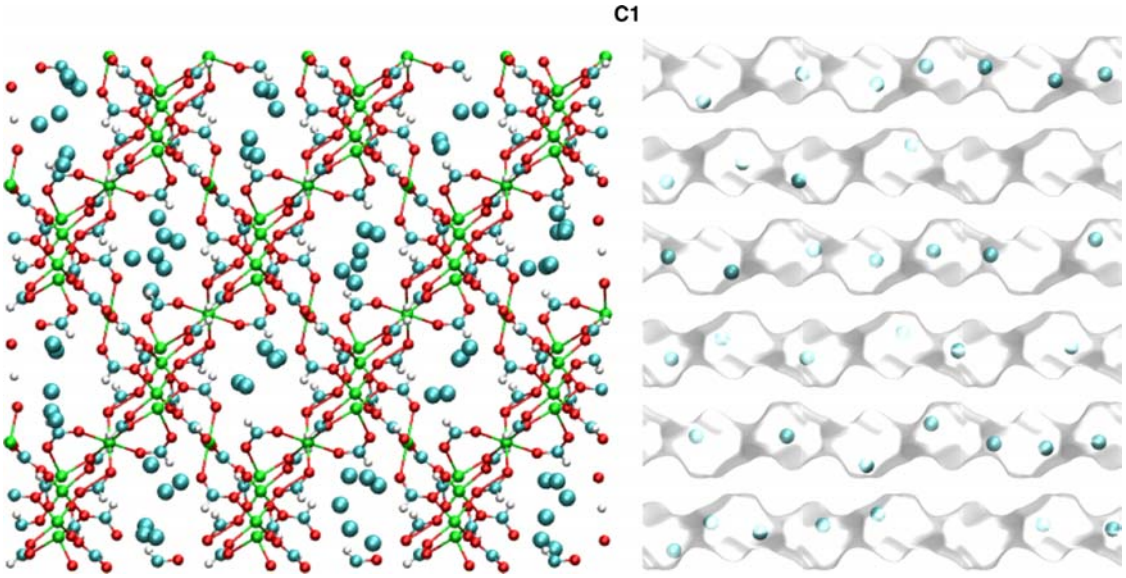

Figure S13.

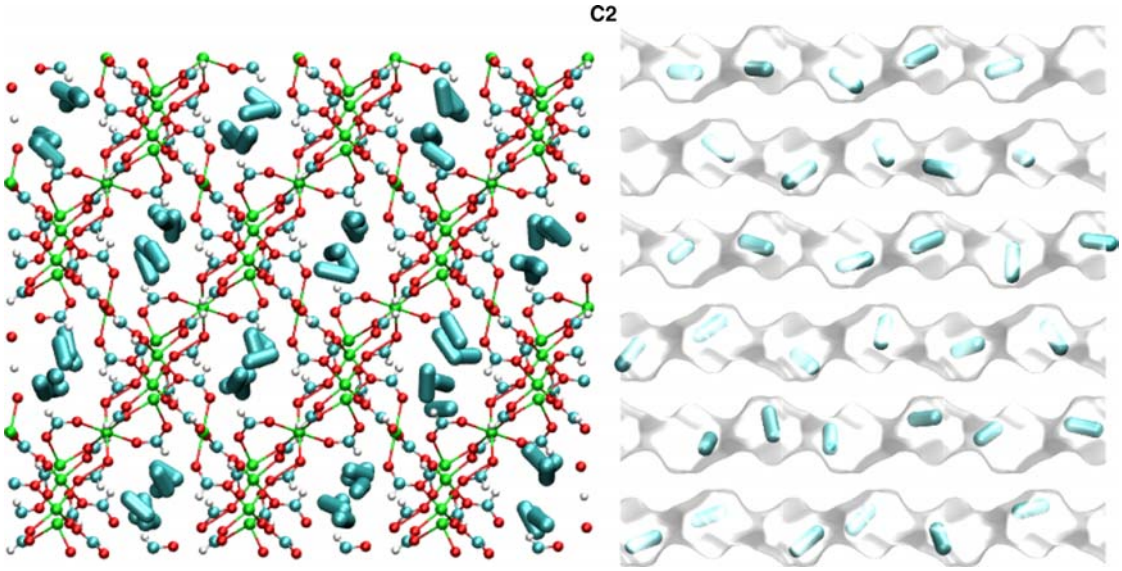

Figure S14.

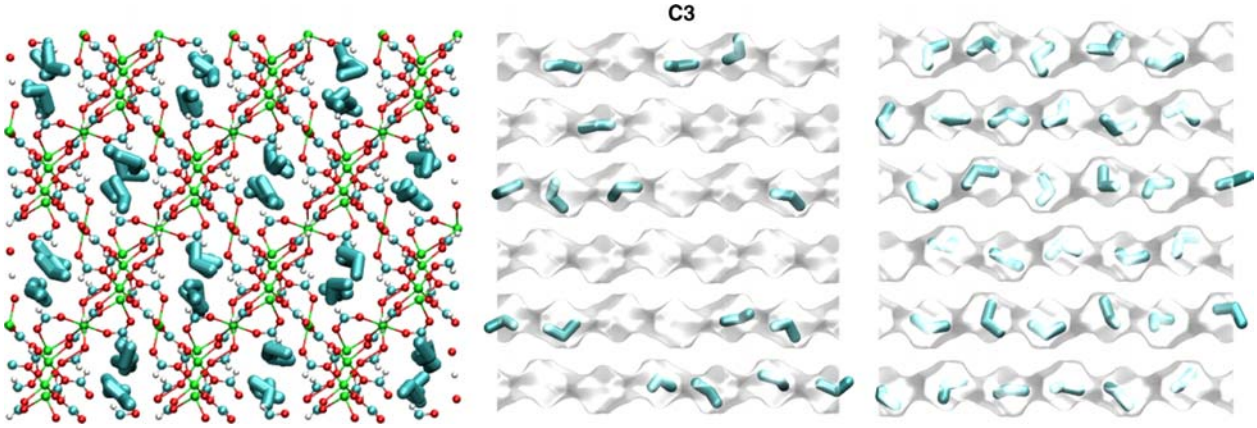

Figure S15.

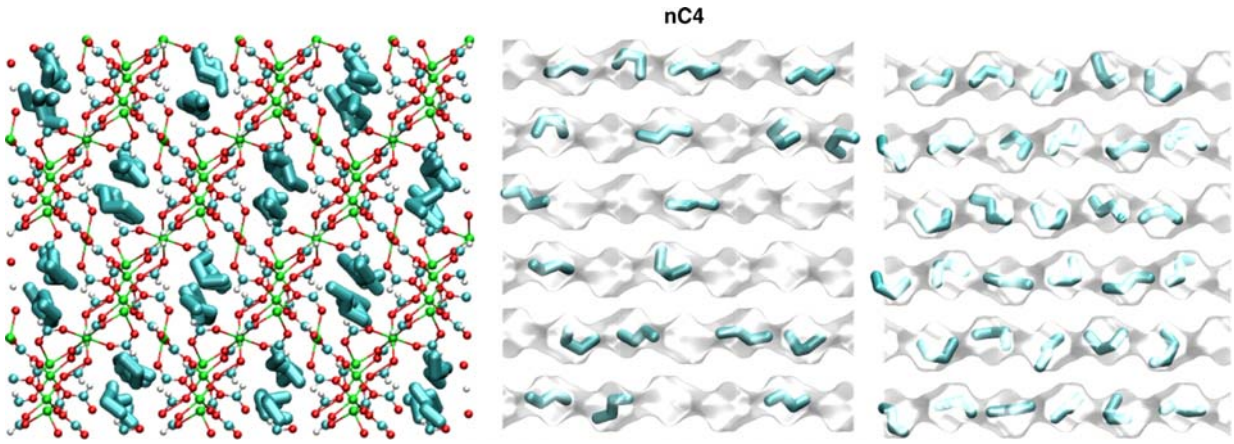

Figure S16.

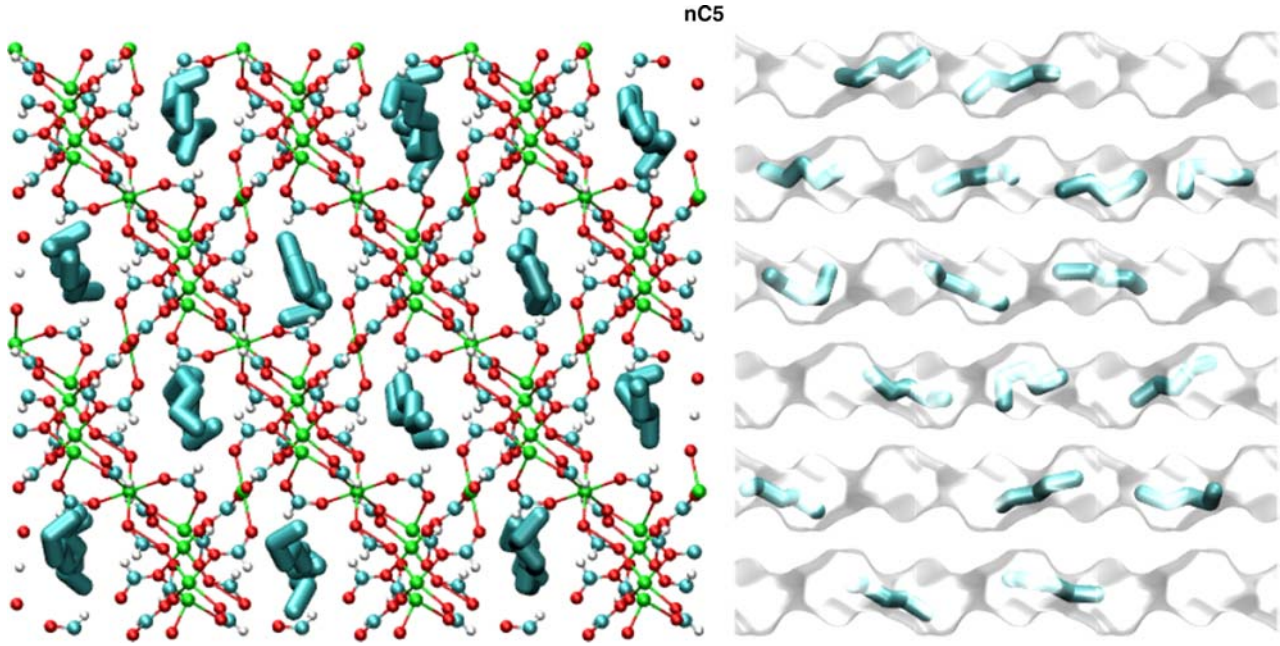

Figure S17.

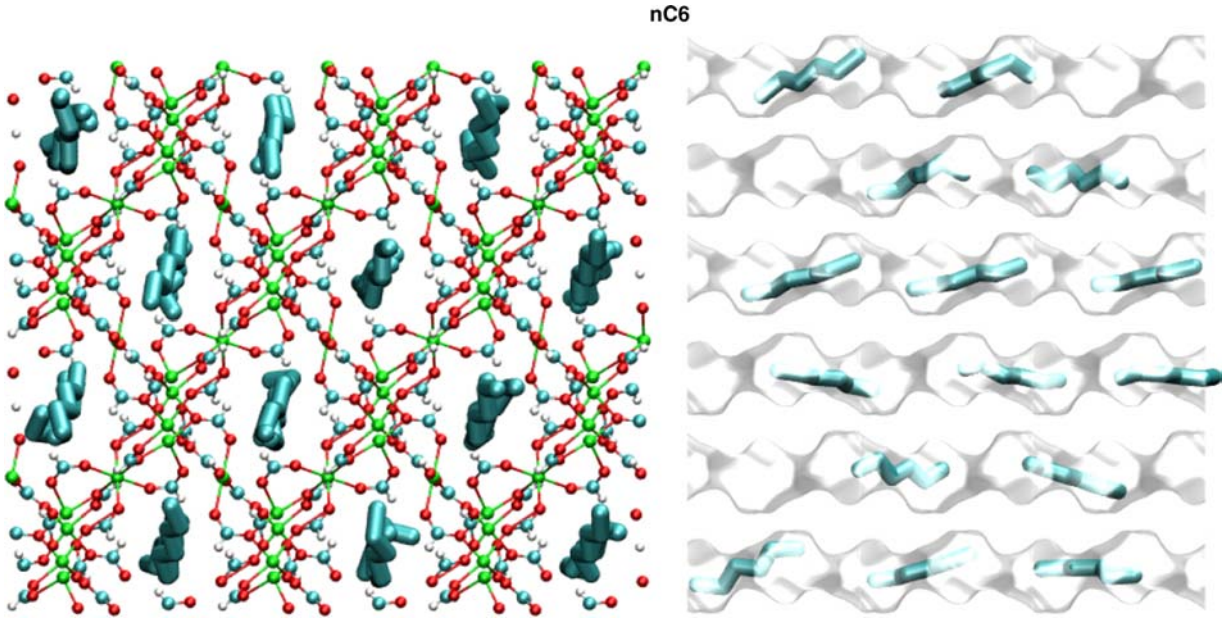

Figure S18.

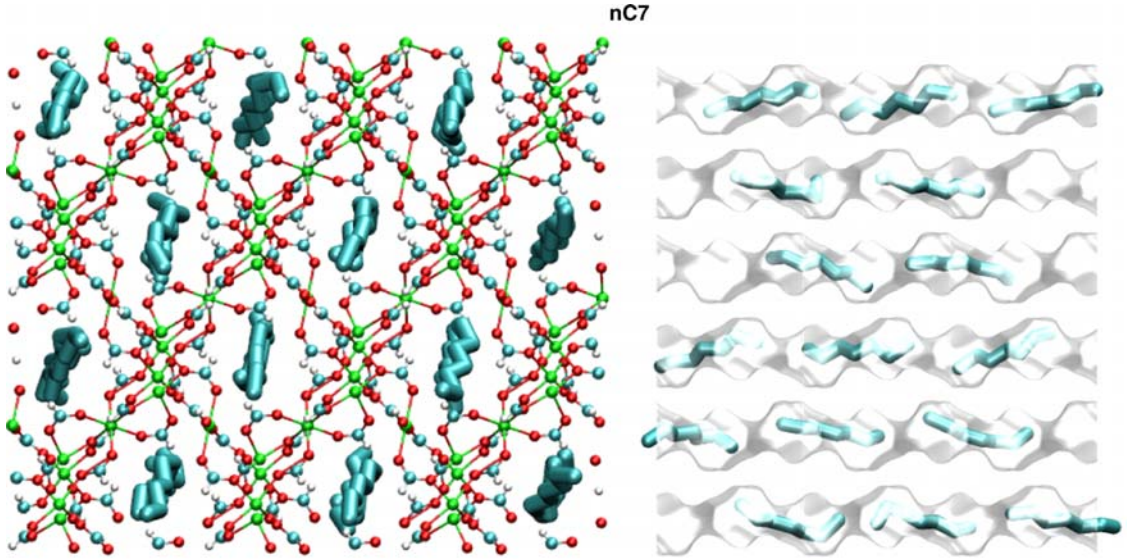

Figure S19.

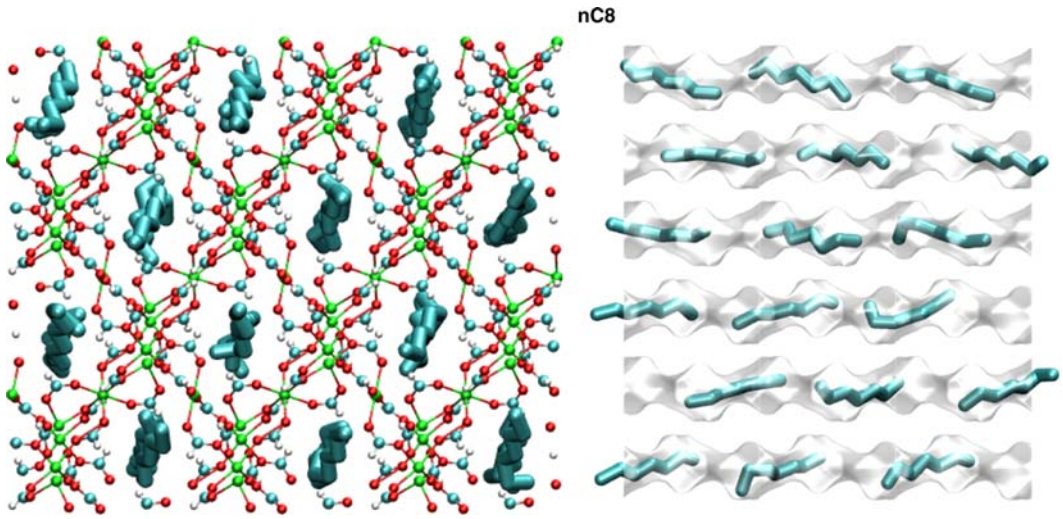

Figure S20.

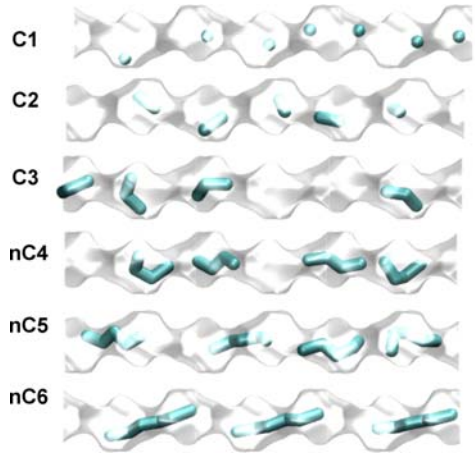

Figure S21.

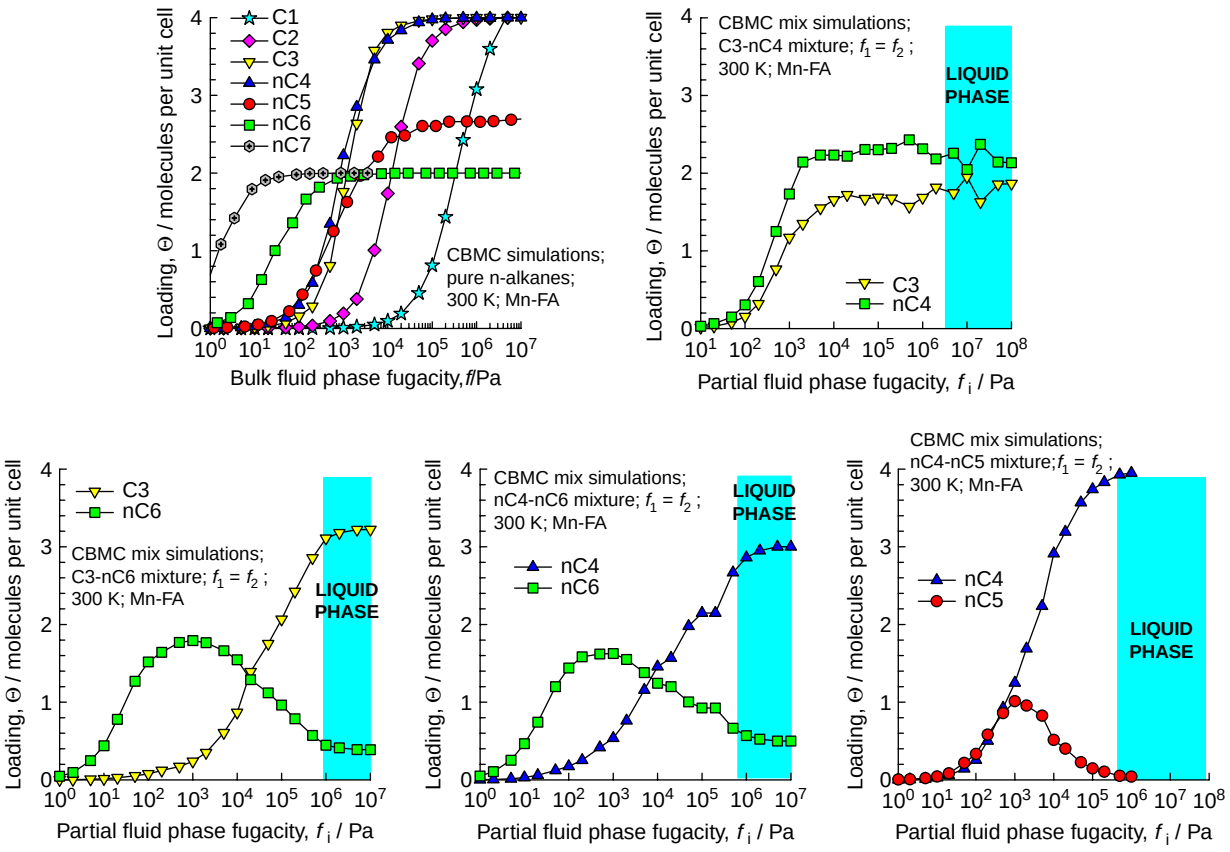

Figure S22.

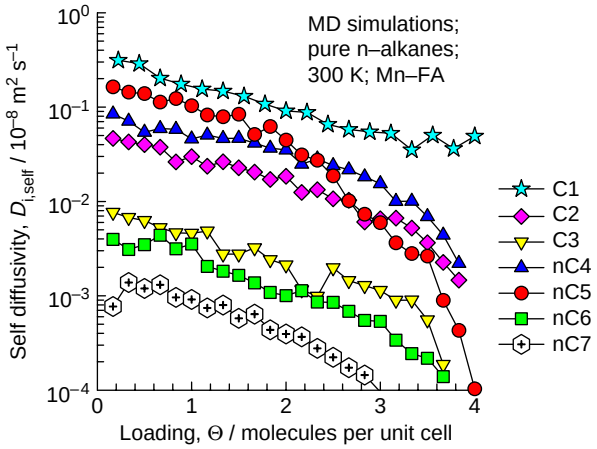

Figure S23.

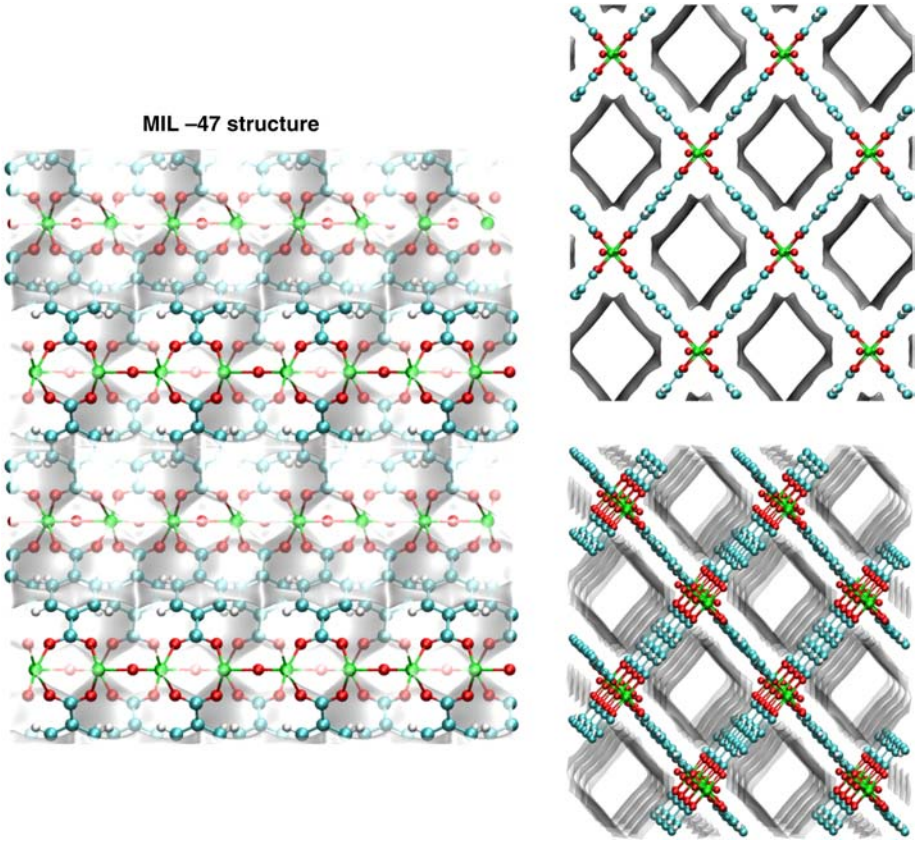

Figure S24.

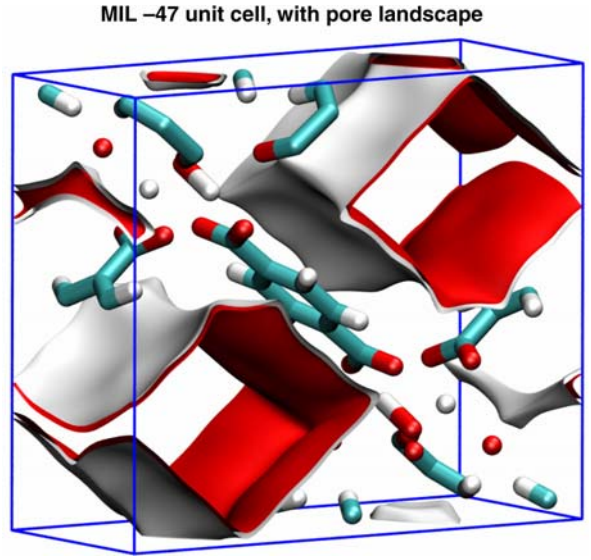

Figure S25.

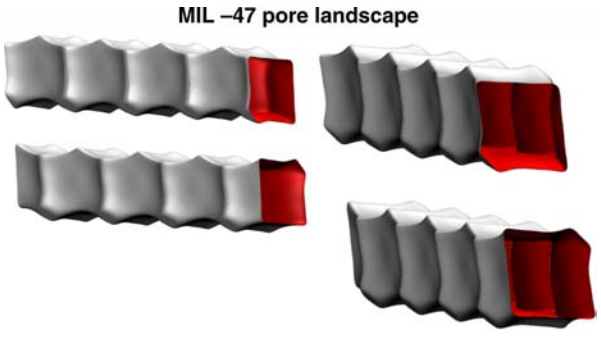

Figure S26.

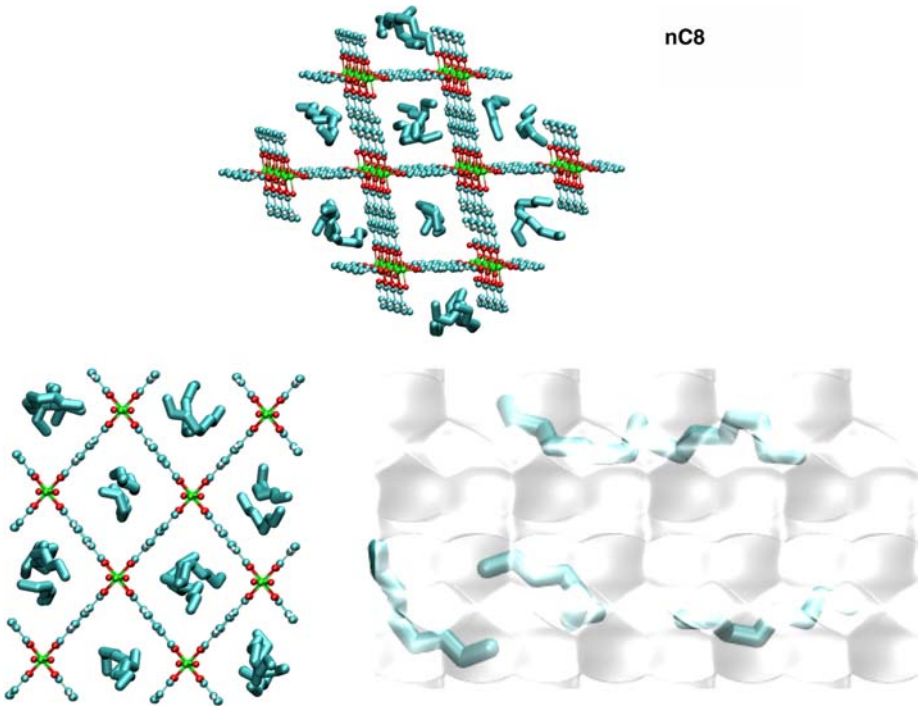

Figure S27.

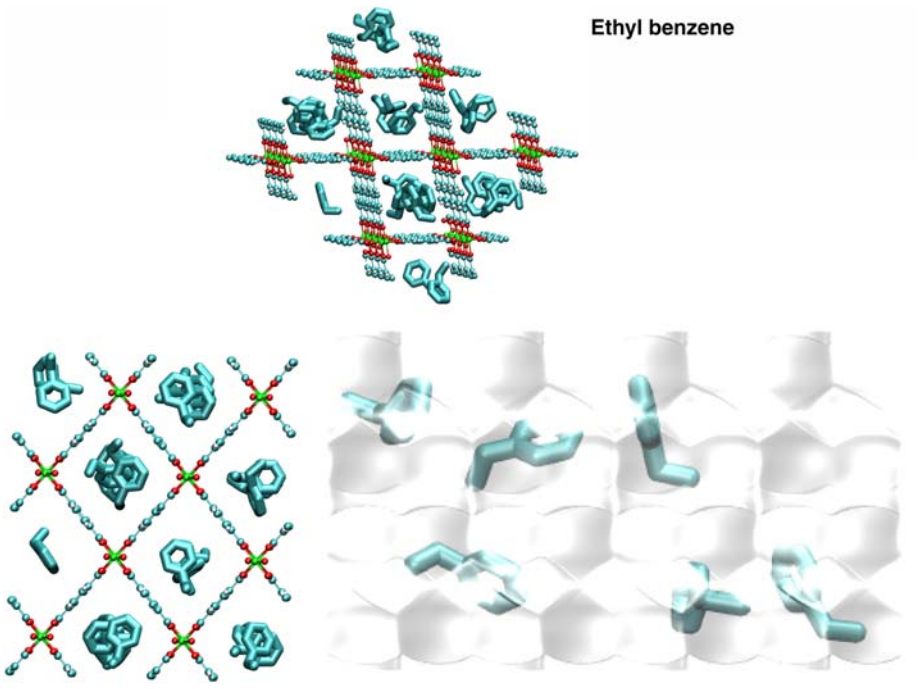

Figure S28.

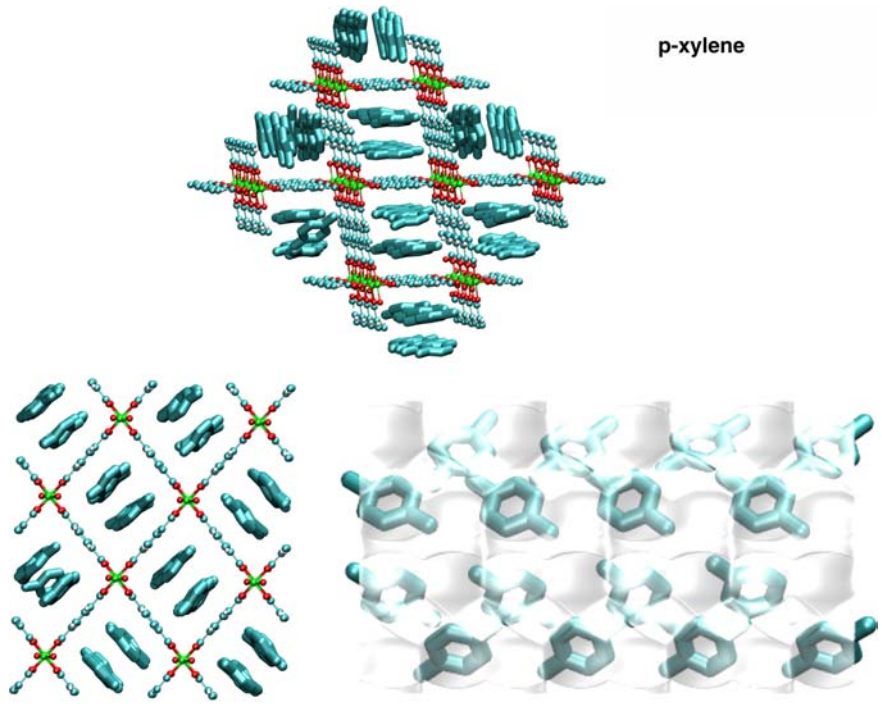

Figure S29.

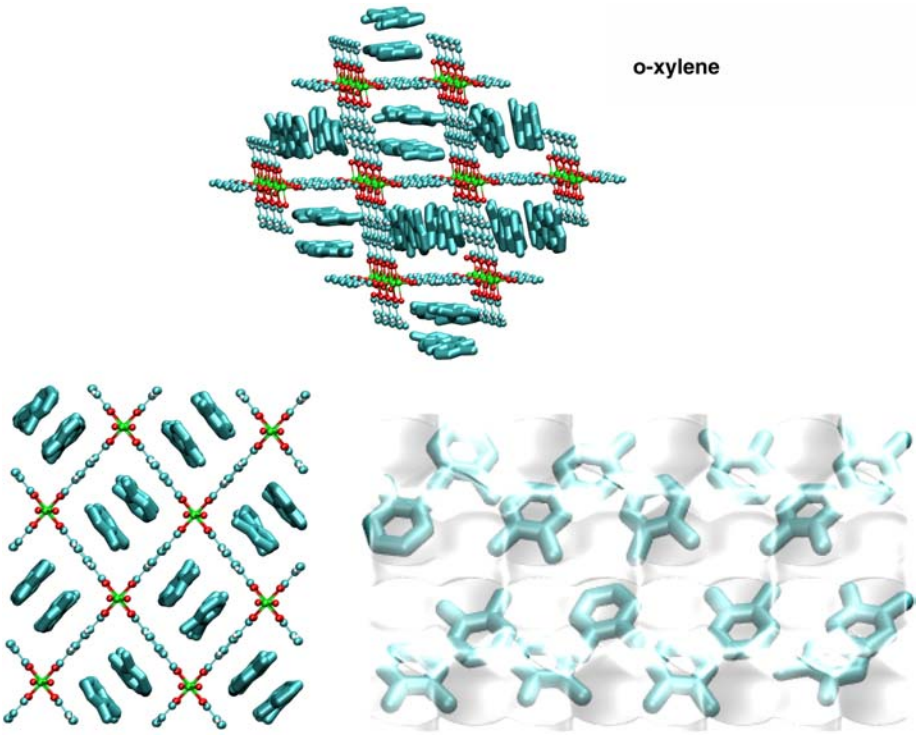

Figure S30.

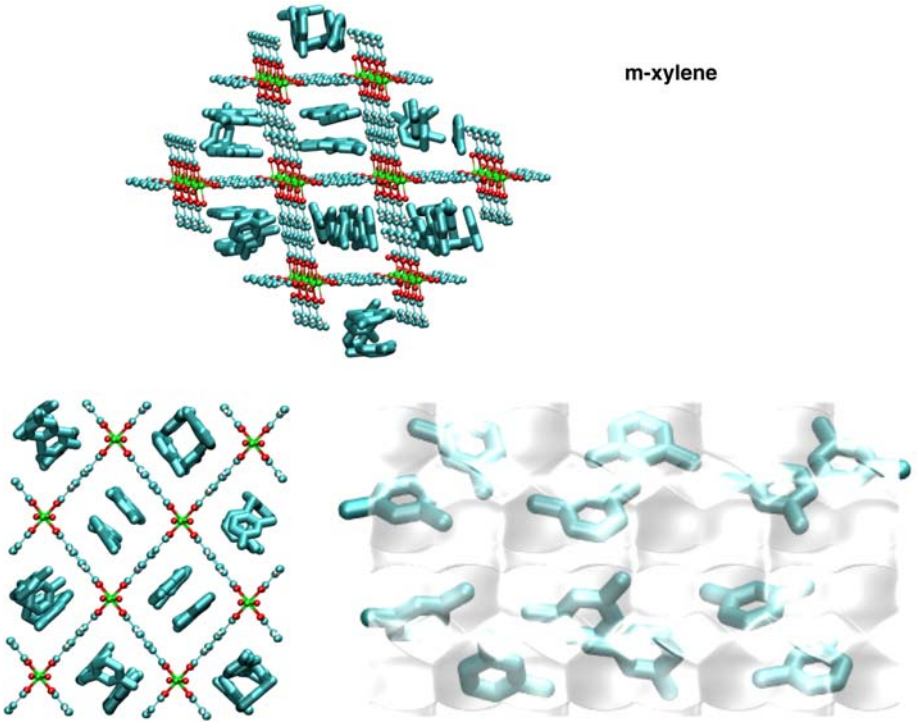

Figure S31.

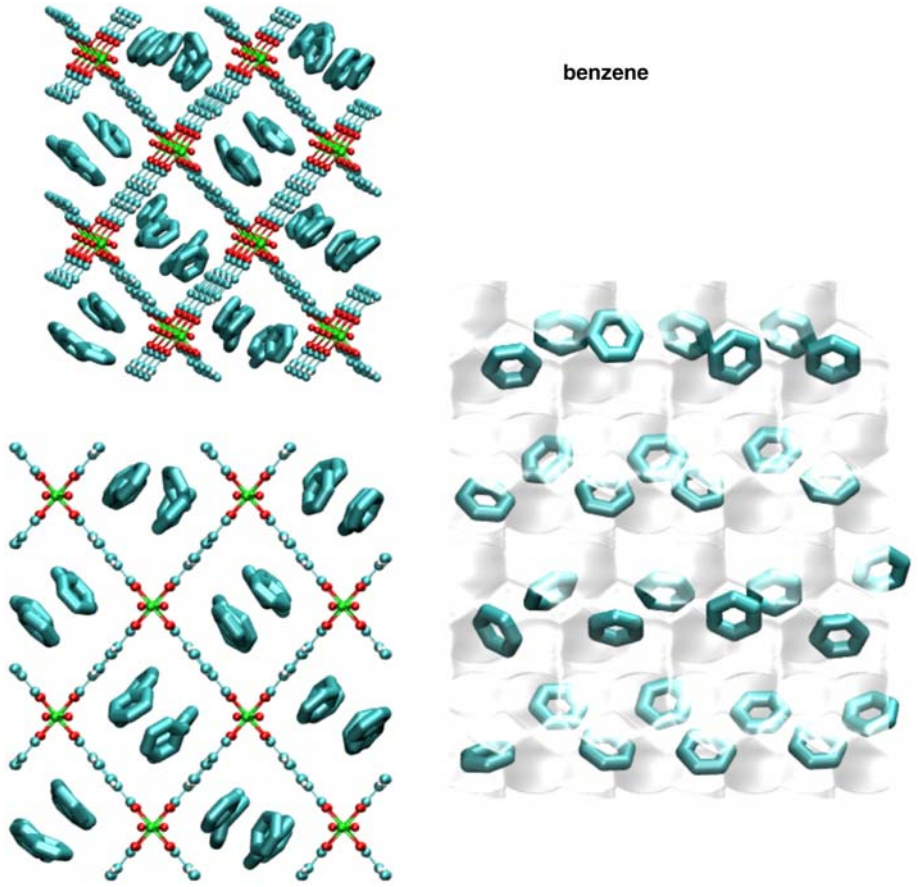

Figure S32.

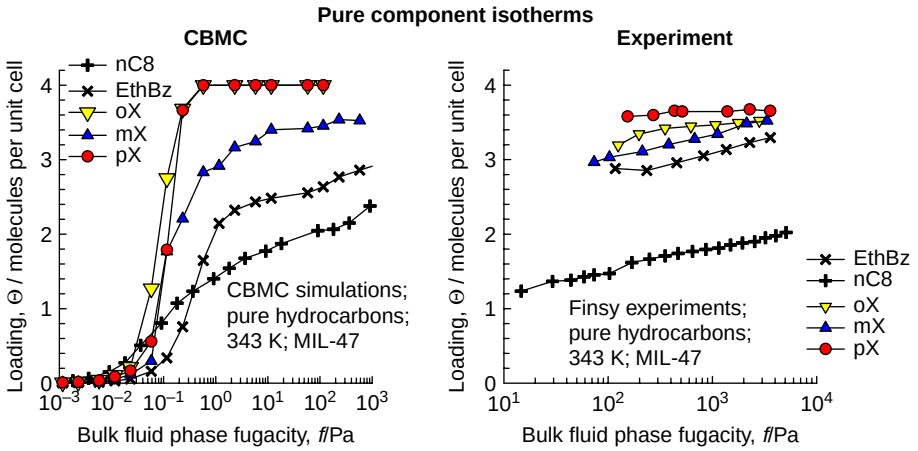

Figure S33.

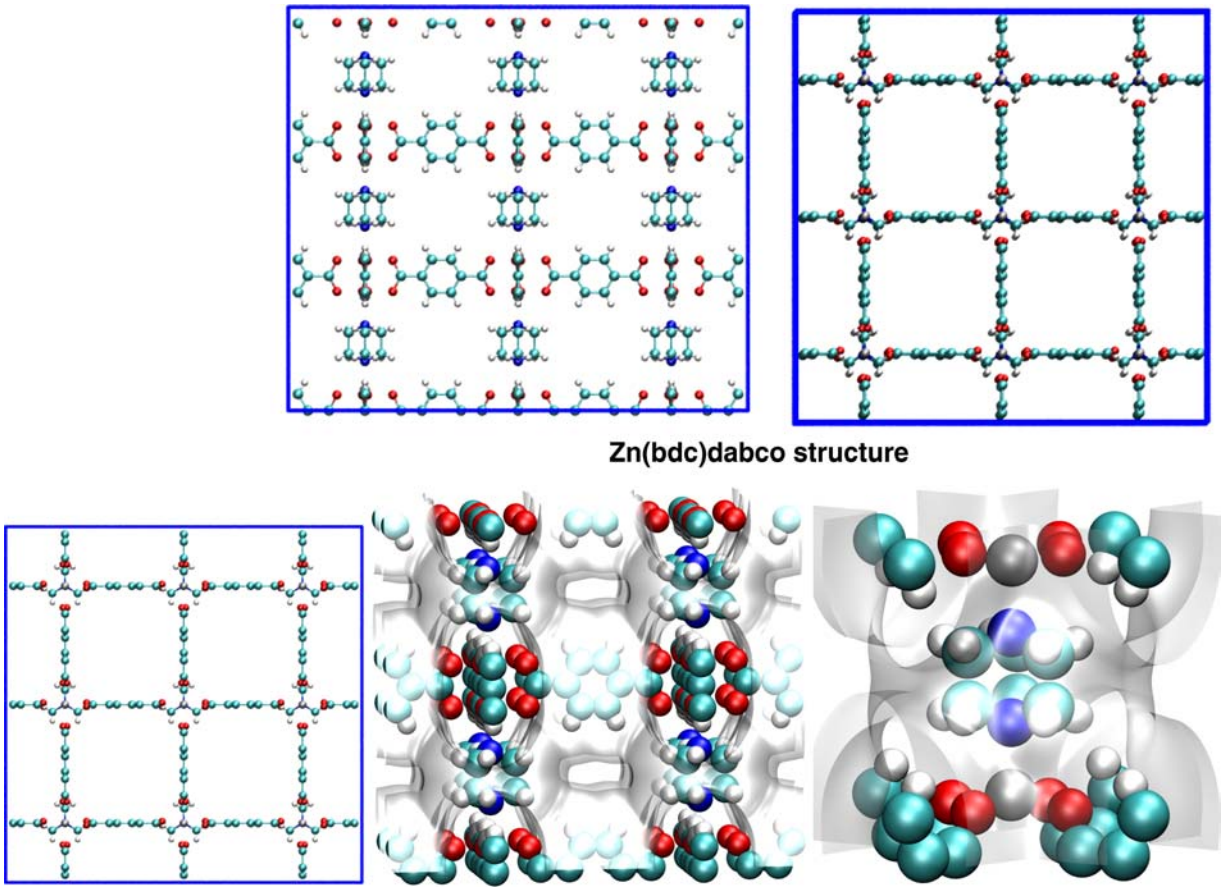

Figure S34.

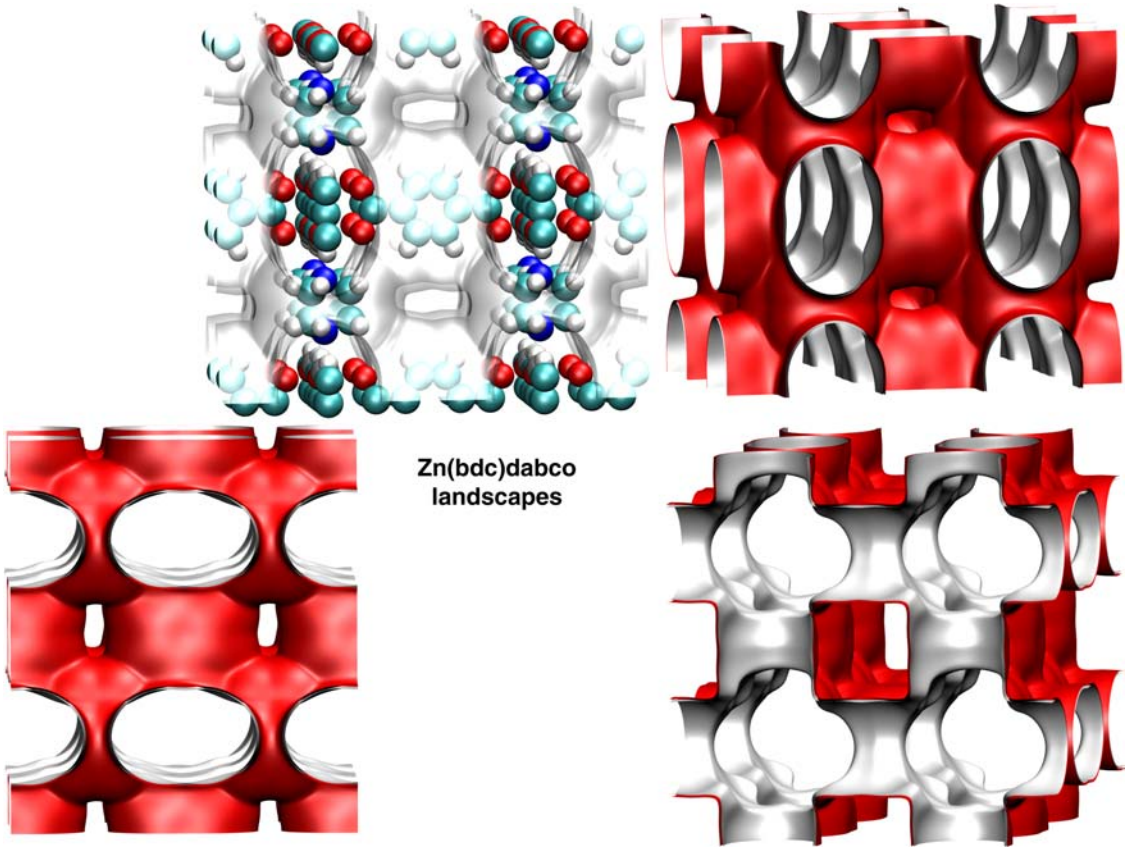

Figure S35.

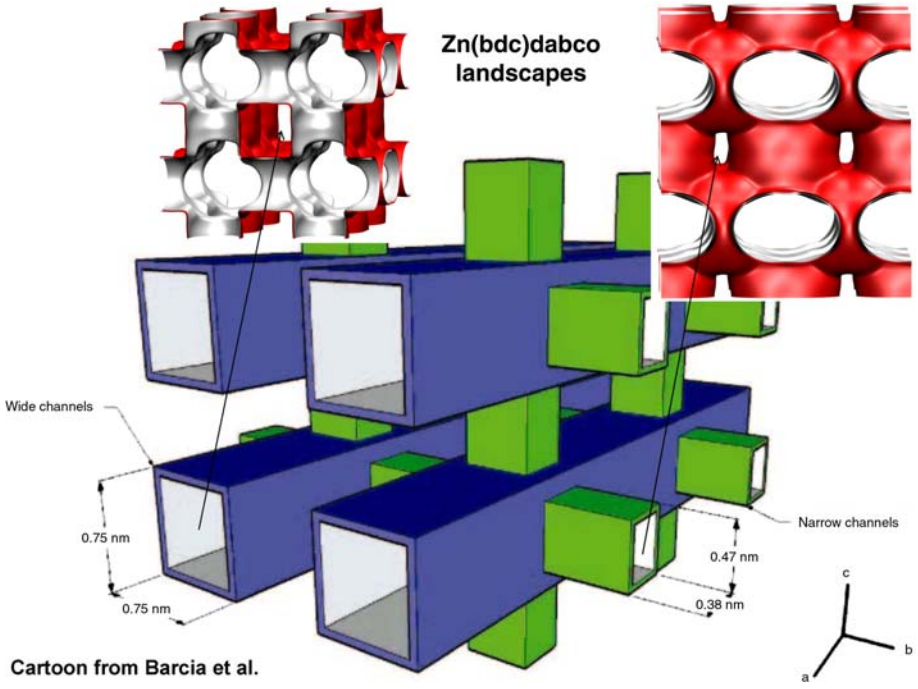

Figure S36.

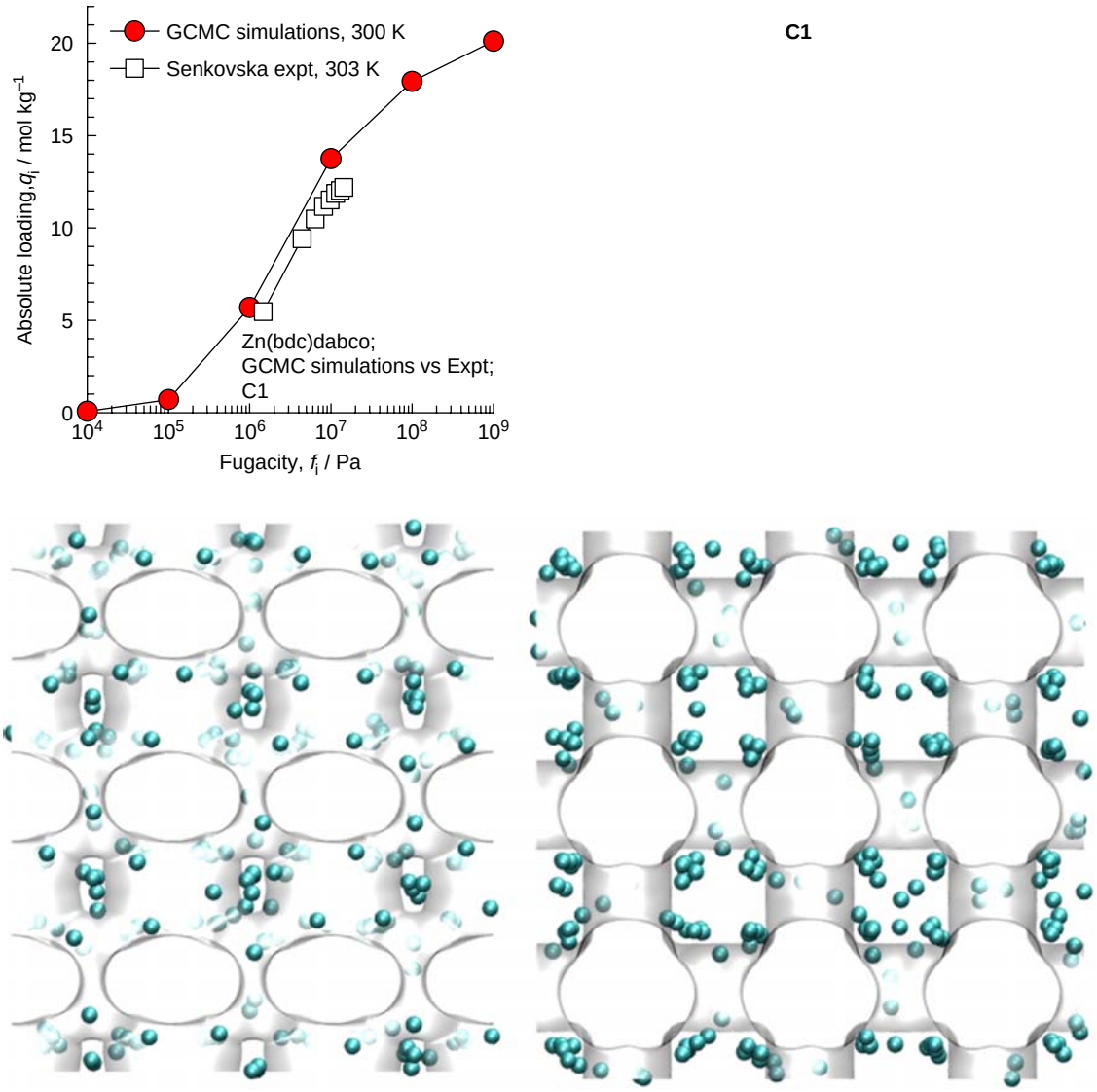

Figure S37. Comparison of simulated isotherm with experimental data of Senkovska and Kaskel [20].

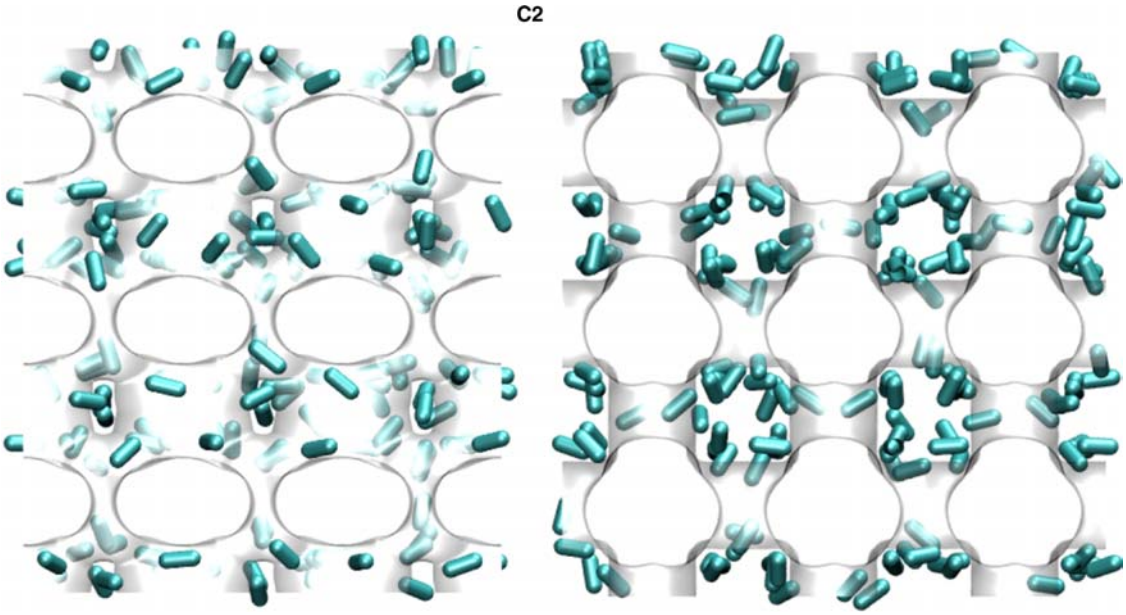

Figure S38.

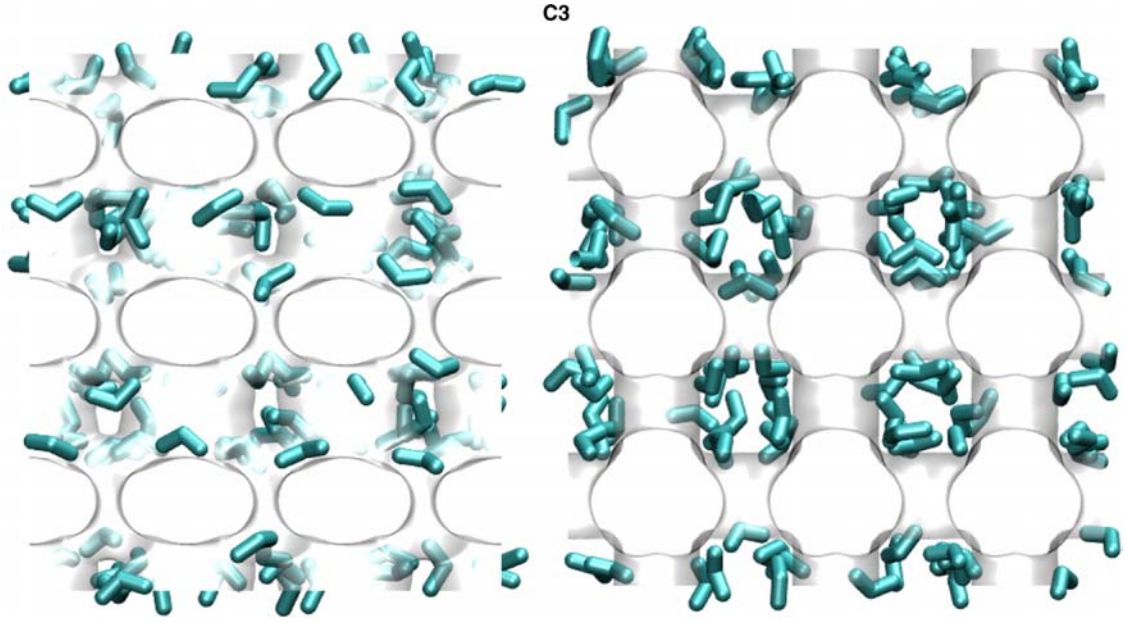

Figure S39.

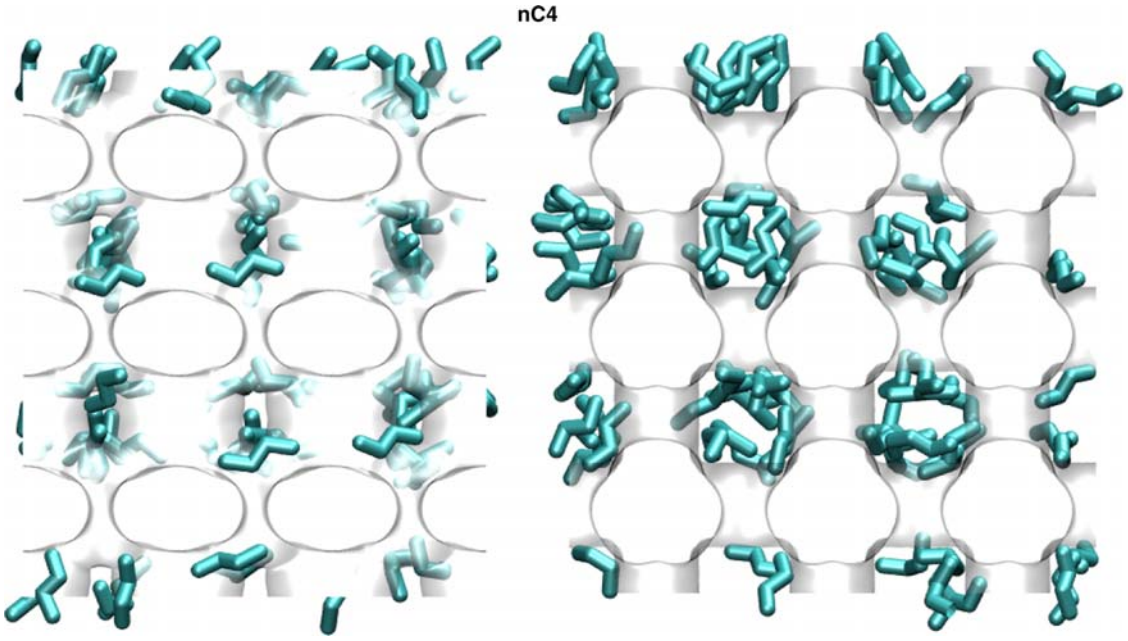

Figure S40.

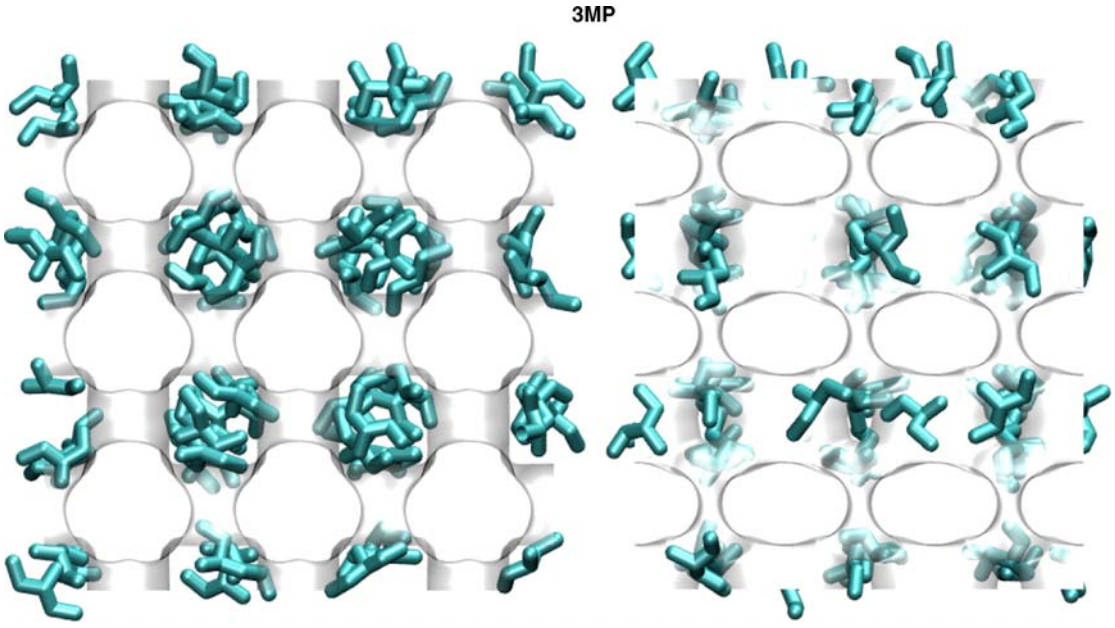

Figure S41.

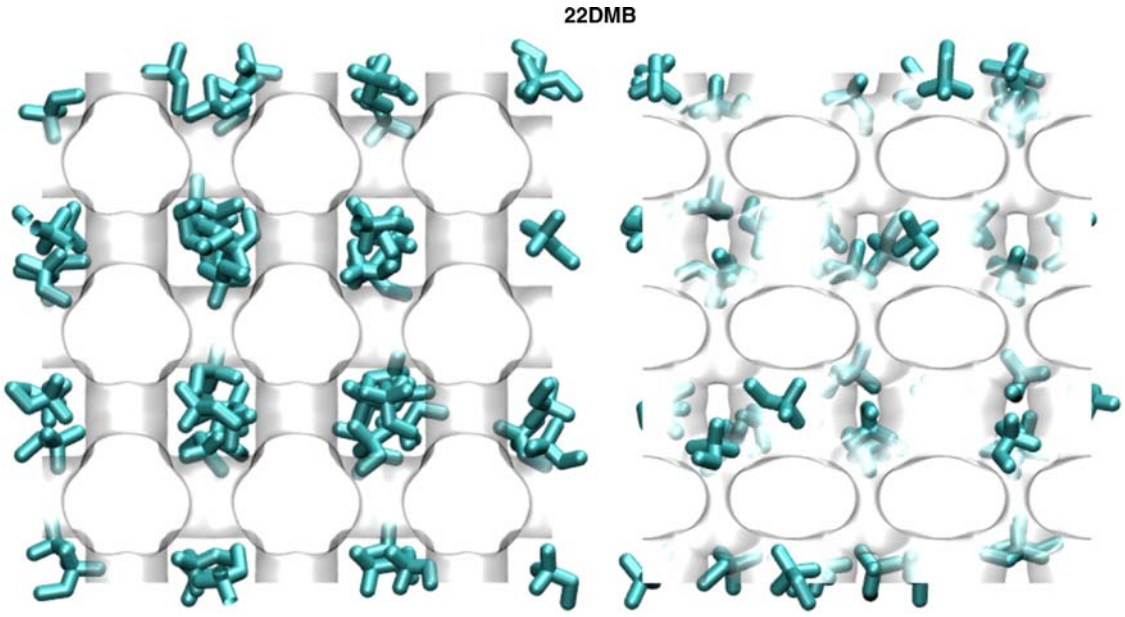

Figure S42.

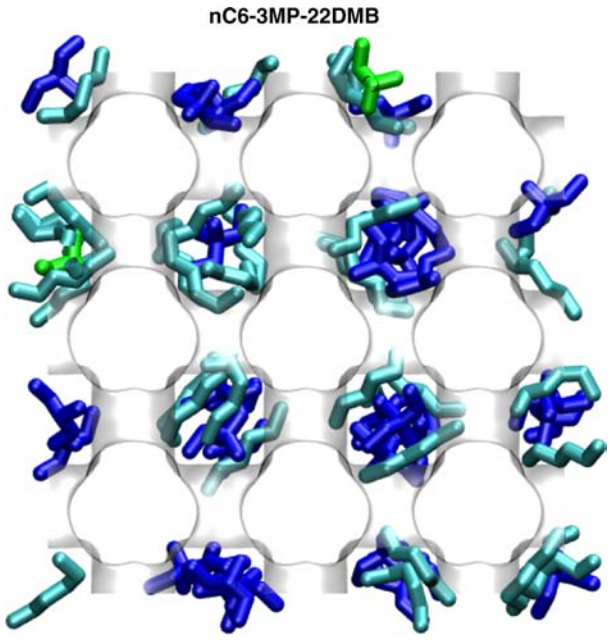

Figure S43.

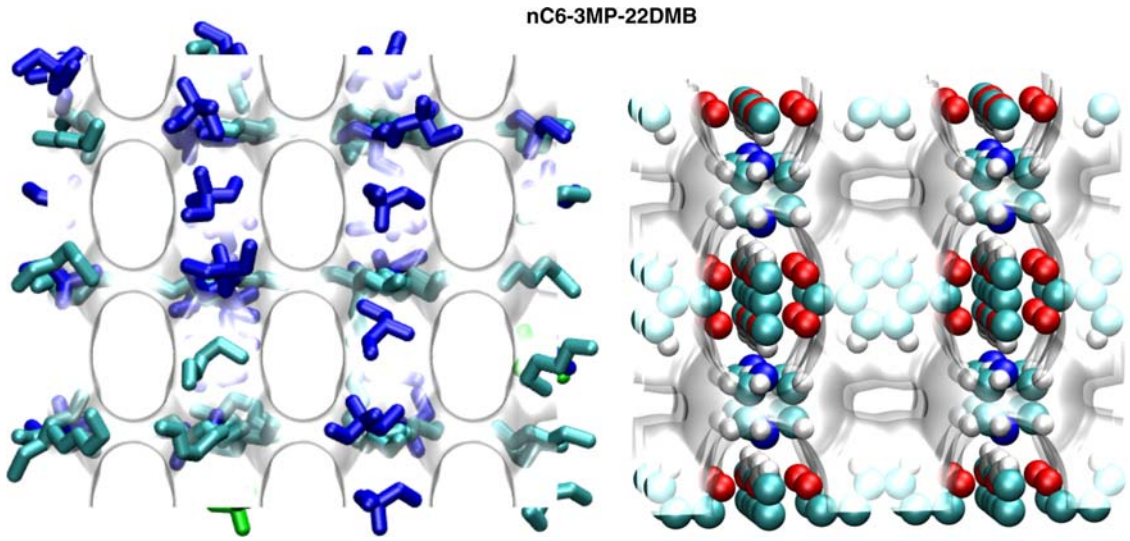

Figure S44.

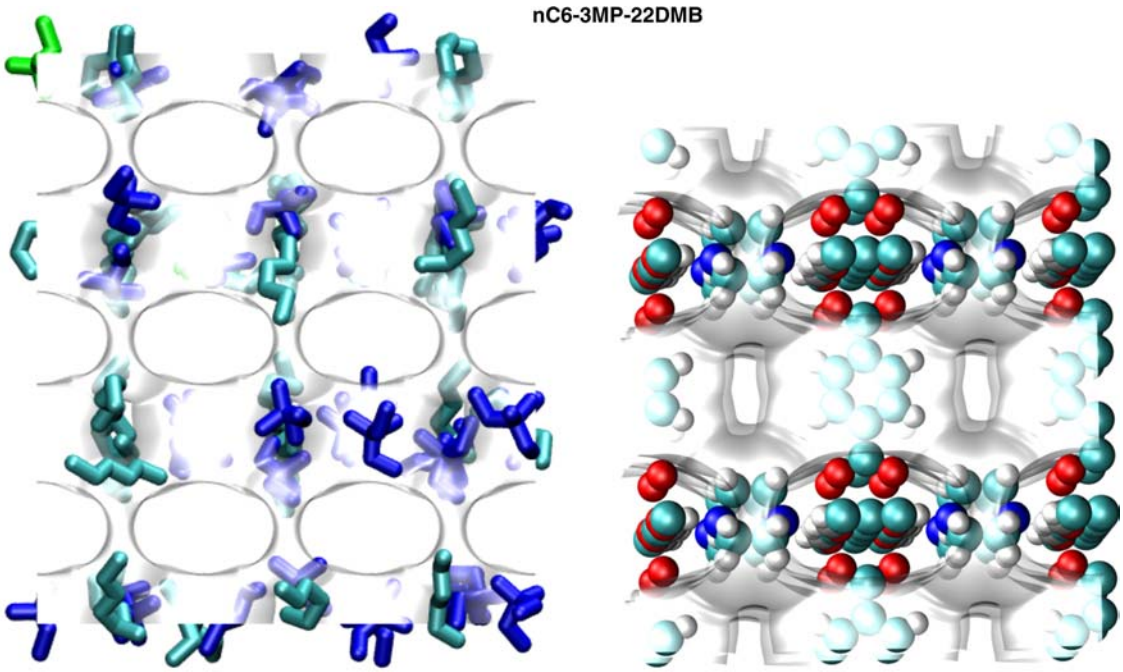

Figure S45.

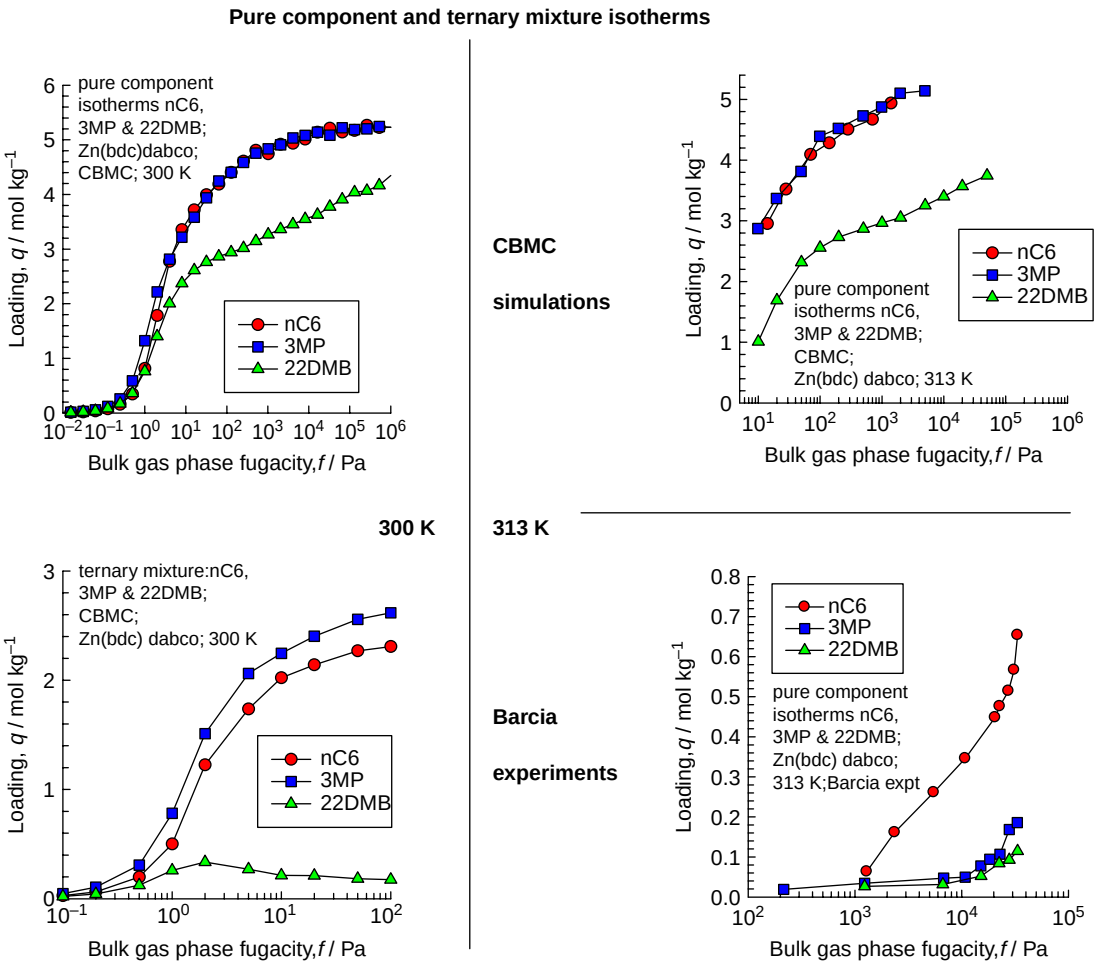

Figure S46.

Acknowledgements

We are grateful to T.J.H. Vlugt, Delft, for providing the BIGMAC code. This code was modified to handle rigid molecular structures and charges, with generous assistance and technical inputs from S. Calero, Seville.

Notation

$D_{i,\mathrm{self}}$ self-diffusivity ($\mathrm{m^2\,s^{-1}}$)
f_i fugacity of species i (Pa)
n_i number of molecules of species i in simulation box, dimensionless
$\mathbf{r}_{l,i}(t)$ position of molecule l of species i at any time t (m)
t time (s)
T absolute temperature (K)

References

[1] K. Li, D.H. Olson, J.Y. Lee, W. Bi, K. Wu, T. Yuen, Q. Xu, and J. Li, *Multifunctional microporous MOFs exhibiting gas/hydrocarbon adsorption selectivity, separation capability and three-dimensional magnetic ordering*, Adv. Funct. Mater. 18 (2008), pp. 2205–2214.

[2] D.N. Dybtsev, H. Chun, S.H. Yoon, D. Kim, and K. Kim, *Microporous manganese formate: a simple metal-organic porous material with high framework stability and highly selective gas sorption properties*, J. Am. Chem. Soc. 126 (2004), pp. 32–33.

[3] P.S. Bárcia, F. Zapata, J.A.C. Silva, A.E. Rodrigues, and B. Chen, *Kinetic separation of hexane isomers by fixed-bed adsorption with a microporous metal-organic framework*, J. Phys. Chem. B 111 (2008), pp. 6101–6103.

[4] J.Y. Lee, D.H. Olson, L. Pan, T.J. Emge, and J. Li, *Microporous metal-organic frameworks with high gas sorption and separation capacity*, Adv. Funct. Mater. 17 (2007), pp. 1255–1262.

[5] L. Alaerts, C.E.A. Kirschhock, M. Maes, M. van der Veen, V. Finsy, A. Depla, J.A. Martens, G.V. Baron, P.A. Jacobs, J.F.M. Denayer, et al., *Selective adsorption and separation of xylene isomers and ethylbenzene with the microporous vanadium(IV) terephthalate MIL-47*, Angew. Chem. Int. Ed. 46 (2007), pp. 4293–4297.

[6] V. Finsy, H. Verelst, L. Alaerts, D. De Vos, P.A. Jacobs, G.V. Baron, J.F.M. Denayer, *Pore-filling-dependent selectivity effects in the vapor-phase separation of xylene isomers on the metal-organic framework MIL-47*, J. Am. Chem. Soc. 130 (2008), pp. 7110–7118.

[7] K. Barthelet, J. Marrot, D. Riou, and G. Férey, *A breathing hybrid organic–inorganic solid with very large pores and high magnetic characteristics*, Angew. Chem. Int. Ed. 41 (2007), pp. 281–284.

[8] J.M. van Baten and R. Krishna, *MD animations of diffusion in nanoporous materials*, University of Amsterdam, Amsterdam, 2008. Available at http://www.science.uva.nl/research/cr/animateMD/.

[9] D. Dubbeldam, S. Calero, T.J.H. Vlugt, R. Krishna, T.L.M. Maesen, and B. Smit, *United atom forcefield for alkanes in nanoporous materials*, J. Phys. Chem. B 108 (2004), pp. 12301–12313.

[10] S. Ban, A. van Laak, P.E. de Jongh, J.P.J.M. van der Eerden, and T.J.H. Vlugt, *Adsorption selectivity of benzene and propene mixtures for various zeolites*, J. Phys. Chem. C 111 (2007), pp. 17241–17248.

[11] A.K. Rappé, C.J. Casewit, K.S. Colwel, W.A. Goddard, and W.M. Skiff, *UFF, a full periodic table force field for molecular mechanics and molecular dynamics simulations*, J. Am. Chem. Soc. 114(1992), pp. 10024–10035.

[12] S.L. Mayo, B.D. Olafson, and W.A. Goddard, *DREIDING: a generic force field for molecular simulations*, J. Phys. Chem. 94 (1990), pp. 8897–8909.

[13] D. Frenkel and B. Smit, *Understanding Molecular Simulations: From Algorithms to Applications*, 2nd ed., Academic Press, San Diego, 2002.

[14] T.J.H. Vlugt, R. Krishna, and B. Smit, *Molecular simulations of adsorption isotherms for linear and branched alkanes and their mixtures in silicalite*, J. Phys. Chem. B 103 (1999), pp. 1102–1118.

[15] D. Dubbeldam, S. Calero, T.J.H. Vlugt, R. Krishna, T.L.M. Maesen, E. Beerdsen, and B. Smit, *Force field parametrization through fitting on inflection points in isotherms*, Phys. Rev. Lett. 93 (2004) 088302.

[16] T.J.H. Vlugt, *BIGMAC*, University of Amsterdam, Amsterdam, 2000. Available at http://molsim.chem.uva.nl/bigmac/.

[17] W. Smith, T.R. Forester, and I.T. Todorov, *The DL_POLY Molecular Simulation Package*, Warrington, England, 2006. Available at http://www.cse.clrc.ac.uk/msi/software/DL_POLY/index.shtml.

[18] SARA, *Computing & Networking Services*, SARA, Amsterdam, 2008. Available at http://subtrac.sara.nl/userdoc/wiki/lisa/description.

[19] D. Dubbeldam, C.J. Galvin, K.S. Walton, D.E. Ellis, and R.Q. Snurr, *Separation and molecular-level segregation of complex alkane mixtures in metal-organic frameworks*, J. Am. Chem. Soc. 130 (2008), pp. 10884–10885.

[20] I. Senkouska and S. Kaskel, *High pressure methane adsorption to the metal-organic frameworks* $Cu_3(btc)_2$, $Zn_2(bdc)_2dabco$, and $Cr_3F(H_2O)_2(bdc)_3$, Micro. Mesopor. Mat. 112 (2008), pp. 108–115.